



CHIP Regulates Aquaporin-2 Quality Control and Body Water Homeostasis

Qi Wu ¹, Hanne B. Moeller,¹ Donté A. Stevens,² Rebekah Sanchez-Hodge,^{2,3} Gabrielle Childers,^{2,3} Marleen L.A. Kortenoeven,¹ Lei Cheng,¹ Lena L. Rosenbaek,^{1,4} Carrie Rubel,² Cam Patterson,⁵ Trairak Pisitkun ^{1,6}, Jonathan C. Schisler,^{2,3} and Robert A. Fenton¹

¹InterPrET Center, Department of Biomedicine, Aarhus University, Aarhus, Denmark; ²McAllister Heart Institute and ³Department of Pharmacology, The University of North Carolina at Chapel Hill, Chapel Hill, North Carolina; ⁴Department of Neuroscience and Pharmacology, University of Copenhagen, Copenhagen, Denmark; ⁵Presbyterian Hospital/Weill-Cornell Medical Center, New York, New York; and ⁶Faculty of Medicine, Chulalongkorn University, Bangkok, Thailand

ABSTRACT

The importance of the kidney distal convoluted tubule (DCT) and cortical collecting duct (CCD) is highlighted by various water and electrolyte disorders that arise when the unique transport properties of these segments are disturbed. Despite this critical role, little is known about which proteins have a regulatory role in these cells and how these cells can be regulated by individual physiologic stimuli. By combining proteomics, bioinformatics, and cell biology approaches, we found that the E3 ubiquitin ligase CHIP is highly expressed throughout the collecting duct; is modulated in abundance by vasopressin; interacts with aquaporin-2 (AQP2), Hsp70, and Hsc70; and can directly ubiquitylate the water channel AQP2 *in vitro*. shRNA knockdown of CHIP in CCD cells increased AQP2 protein $t_{1/2}$ and reduced AQP2 ubiquitylation, resulting in greater levels of AQP2 and phosphorylated AQP2. CHIP knockdown increased the plasma membrane abundance of AQP2 in these cells. Compared with wild-type controls, CHIP knockout mice or novel CRISPR/Cas9 mice without CHIP E3 ligase activity had greater AQP2 abundance and altered renal water handling, with decreased water intake and urine volume, alongside higher urine osmolality. We did not observe significant changes in other water- or sodium-transporting proteins in the gene-modified mice. In summary, these results suggest that CHIP regulates AQP2 and subsequently, renal water handling.

J Am Soc Nephrol 29: 936–948, 2018. doi: <https://doi.org/10.1681/ASN.2017050526>

The ability of the kidney to maintain body water balance and the systemic concentrations of various ions is critical for mammals to survive under varying fluid and dietary intakes. To allow these homeostatic processes to be performed simultaneously, the renal tubule has developed

Significance Statement

The distal convoluted tubule (DCT) and cortical collecting duct (CCD) play unique and diverse roles in water and electrolyte handling, but little is known about the unique subset of regulatory proteins in these cells. This manuscript combines proteomics and bioinformatics to identify differentially expressed proteins in the DCT and CCD under various physiological stimuli. The different regulatory proteins within each cell type likely infer their unique transport properties. We show that one regulatory protein highly expressed in the CCD, the E3 ubiquitin ligase CHIP, modulates the function of the water channel aquaporin-2 and plays a role in renal water handling. Pharmaceutical modulation of CHIP function could be a novel approach to treat various water balance disorders.

Received May 16, 2017. Accepted November 14, 2017.

J.C.S. and R.A.F. contributed equally to this work.

Published online ahead of print. Publication date available at www.jasn.org.

Correspondence: Dr. Robert A. Fenton, Department of Biomedicine, Aarhus University, Wilhelm Meyers Allé 3, Building 1233, DK-8000 Aarhus C, Denmark. Email: robert.a.fenton@biomed.au.dk

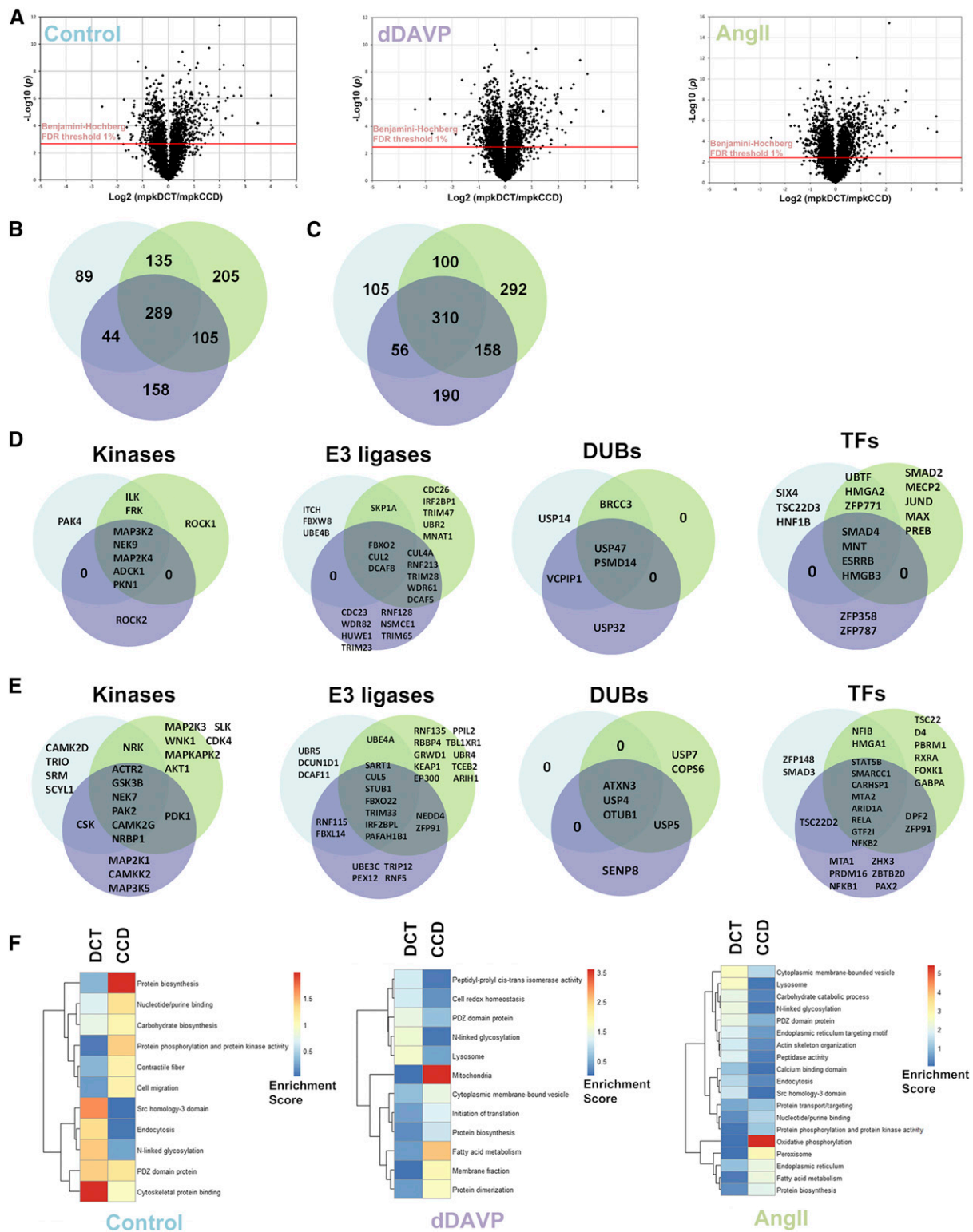


Figure 1. Quantitative proteomic and bioinformatics of mpkDCT and mpkCCD cells reveal cell- and treatment-specific kinases, E3 ligases, deubiquitylases (DUBs), transcription factors, and enriched functional annotations. (A) Volcano plots of quantification between mpkDCT and mpkCCD under three conditions. (A) BH-FDR 1% cutoff was used to select the differential proteome between these two cell types. (B) Number of mpkDCT-specific proteins under three conditions. (C) Number of mpkCCD-specific proteins under three conditions. (D) mpkDCT-specific kinases, E3 ligases, DUBs, and TFs under three conditions. (E) mpkCCD-specific kinases, E3 ligases, DUBs, and TFs under three conditions. (F) Heat maps of mpkDCT and mpkCCD cells illustrating highly enriched functional annotations under three conditions.

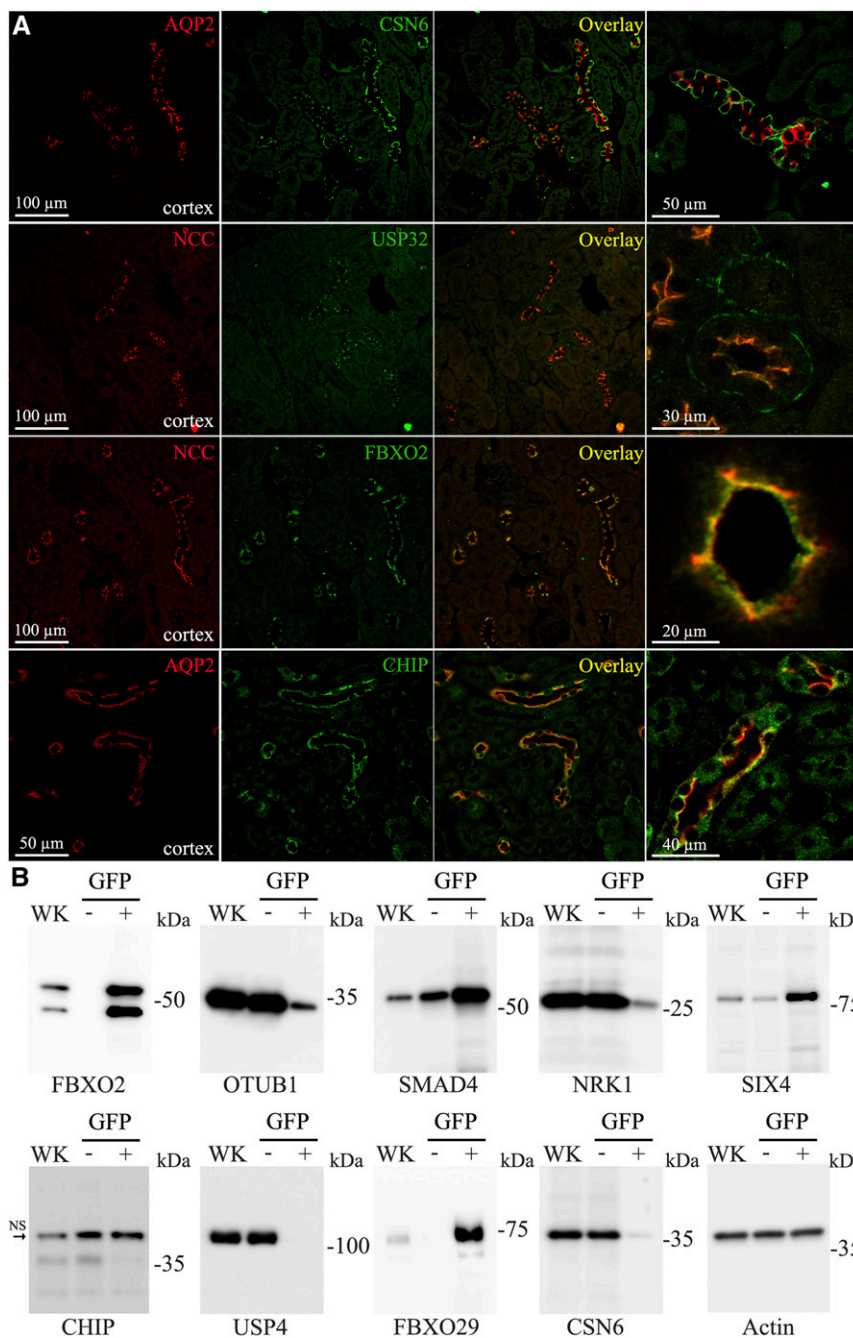


Figure 2. Confirmation of DCT or CCD enriched proteins *in vivo*. (A) Confocal images of mouse kidney sections immunolabeled for COP9 Signalosome Subunit 6 (CSN6), USP32, FBXO2, and CHIP alongside the DCT- or CCD-expressed proteins NCC or AQP2, respectively. (B) Immunoblotting of purified DCT cells (mpkDCT) and CCD cells (mpkCCD) for various proteins. FBXO2, SMAD4, SIX4, and FBXO29 are abundant in isolated DCT cells, whereas the mpkCCD-enriched proteins NRK1, USP4, CSN6, and CHIP are predominantly identified in the GFP⁻ fraction (representing non-DCT cells).

specialized epithelial cells that allow independent regulation of water and solute excretion. Two examples of these epithelial cells are the cells of the distal convoluted tubule (DCT) and principal cells of the cortical collecting duct (CCD).¹

The unique functions of DCT and CCD cells are inferred, at least in part, by the selective expression and regulation of a variety of different membrane-associated transport proteins. For example, in DCT cells, there is expression of the divalent cation transporters TRPV5, NCX1, and TRMP6 that are essential for maintaining calcium and magnesium homeostasis and the thiazide-sensitive NaCl cotransporter NCC that plays a central role in regulated NaCl reabsorption.² In contrast, CCD principal cells express a variety of aquaporin (AQP) water channels that help maintain body water balance.³

Despite differing transporter profiles, the functions of DCT and CCD principal cells are under tight regulation by similar hormones, such as aldosterone, angiotensin II (AngII), and vasopressin (AVP).^{2,4-6} Furthermore, transport proteins, such as the epithelial sodium channel, the chloride channel CLC-K2, and the potassium channel ROMK, are localized to both cell types.^{2,6-8} Therefore, critical to understanding how DCT and CCD cells maintain a unique transport profile but respond to similar hormones is knowledge of the regulatory proteins within each cell type that are responsible for both modulating cell-specific gene expression and also, determining hormone-selective regulatory responses within individual cells.

In this study, to identify novel and unique regulatory proteins important for modulation of DCT and CCD function, we determined the differential proteome of kidney DCT cells (mpkDCT) and CCD cells (mpkCCD), which are extensively characterized models of DCT cells and CCD principal cells.⁹⁻¹² After extensive bioinformatics and confirmatory *in vivo* studies, we characterized the role of the CCD-enriched E3 ubiquitin ligase C terminus of Hsc70 Interacting Protein (CHIP) for modulating the function of AQP2 and subsequent renal water handling.

RESULTS

mpkDCT and mpkCCD Differential Proteome Analyses

LC-MS/MS shotgun proteomics was used to investigate the differential proteome between mpkDCT and mpkCCD under basal, [deamino-Cys1, D-Arg8] vasopressin (dDAVP; a synthetic analog of AVP), and AngII conditions (Supplemental Figure 1). Of 4000 quantifiable proteins in each condition, 1101, 1294, and 1566

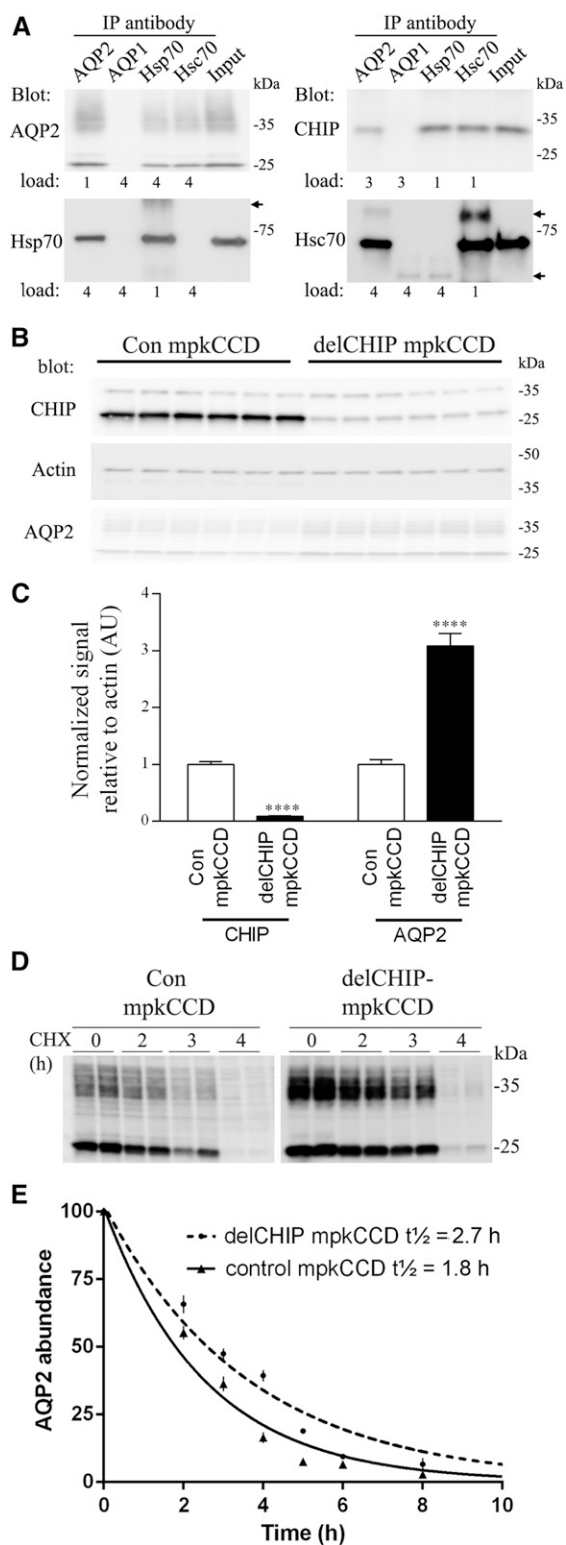


Figure 3. CHIP interacts with AQP2 and modulates its abundance. (A) Coimmunoprecipitation of AQP2, Hsc70, Hsp70, and CHIP from mpkCCD14 cells. “Load” indicates the relative ratio of sample loaded on immunoblots. Arrows indicate nonspecific Igs. IP, immunoprecipitation. (B) Representative immunoblot showing increased AQP2 levels in A4delCHIP cells relative to control

proteins passed the Benjamini–Hochberg FDR threshold of 1% under basal, dDAVP, and AngII conditions, respectively (<http://interpretdb.au.dk/database/DCTCCDcomparison/Control.html>, <http://interpretdb.au.dk/database/DCTCCDcomparison/dDAVP.html>, and <http://interpretdb.au.dk/database/DCTCCDcomparison/AngII.html>) (Figure 1A, Supplemental Table 1; Supplemental Tables 1–6 can be downloaded from <http://interpretdb.au.dk/database/DCTCCDcomparison/download.html>). Five hundred ninety-four proteins were present in all conditions, representing the shared and unchanged portion of the mpkDCT and mpkCCD proteome. Another 287 proteins of higher abundance were identified in mpkDCT cells, and 307 proteins were identified in mpkCCD cells (Supplemental Table 2); 1025 proteins were specific for mpkDCT (Supplemental Material discusses selection criteria), and 1211 proteins were specific for mpkCCD (Figure 1, B and C, Supplemental Table 3). Comparison of specific proteins with a mouse kinome database (<http://kinase.com/kinbase>) determined that ten and 22 kinases are selective for mpkDCT and mpkCCD cells, respectively (Figure 1, D and E); 24 and 29 proteins with known E3 ligase or E3 ligase adapter activity and six and seven proteins with deubiquitylase activity^{13,14} were identified in mpkDCT and mpkCCD cells, respectively (Figure 1, D and E). In addition several transcription factors were identified (Figure 1, D and E), but cross reference of these with matrix families for characteristic genes expressed in the DCT or CCD (Supplemental Table 4) indicated that only one matrix family, V\$SIXF, seemed to be highly specific. The abundances of several proteins were confirmed using Western blotting of equal protein equivalents (Supplemental Figure 2) isolated from a different cohort of cells cultured under similar conditions (Supplemental Figures 3–5). Abundance ratios derived from semiquantitative immunoblotting or MS were highly similar, with Spearman correlations of 0.92, 0.57, and 0.93 under basal, dDAVP, and AngII conditions, respectively (Supplemental Figure 6).

Gene Ontology and Functional Annotation Analyses

Panther gene ontology term molecular function analysis highlighted major processes highly enriched in mpkDCT and mpkCCD cells (Supplemental Figure 7). The Database for Annotation, Visualization and Integrated Discovery tool identified 11, 12, and 19 functional processes in basal, dDAVP, and AngII conditions that were highly enriched in at least one cell type (Figure 1F). For example,

mpkCCD cells. (C) Summary of abundance data from three independent experiments. Asterisks indicate significance relative to control mpkCCD cells. **** $P < 0.001$. (D) Representative AQP2 immunoblot from cells treated with cycloheximide (CHX) for various time periods shows that the increased AQP2 levels in A4delCHIP cells are due to reduced AQP2 degradation. Samples are on the same immunoblot with the same exposure time, and the break is for illustration purposes only. (E) Summarized CHX data fitted using nonlinear regression and a one-phase exponential decay equation. AQP2 abundance is normalized to the zero time point. Values are obtained from four independent experiments, with $n = 3–6$ for each individual time point.

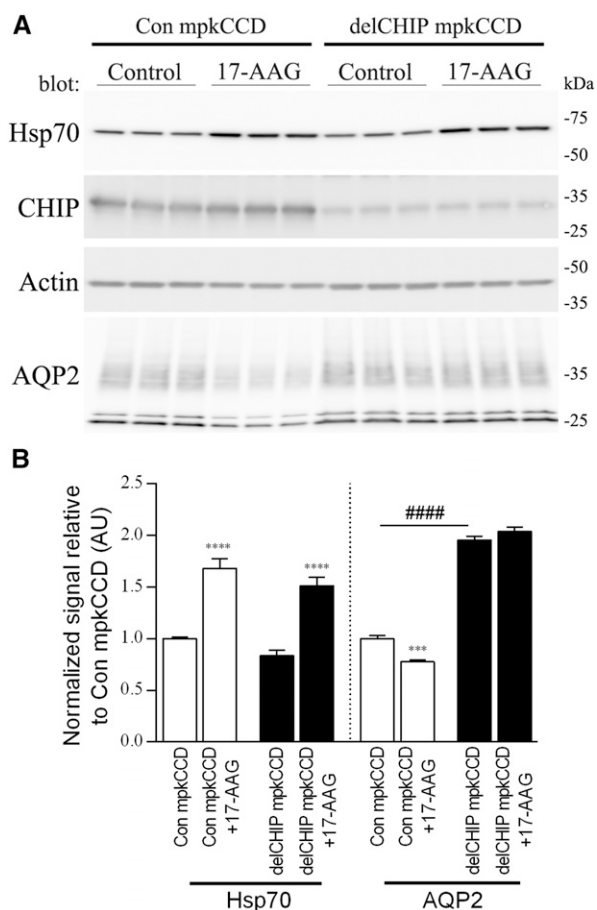


Figure 4. Inhibition of Hsp90 in control and delCHIP mpkCCD cells support a role of CHIP in AQP2 degradation. (A) Representative immunoblots from mpkCCD cells treated with the Hsp90 inhibitor 17-AAG. (B) Summary of 17-AAG data from three independent experiments. Asterisks indicate significance relative to control conditions within an individual cell line. *** $P < 0.001$; **** $P < 0.001$; #### $P < 0.001$ (significance between cell lines).

processes linked to PDZ domain proteins and *N*-linked glycosylation were enriched in mpkDCT cells, whereas protein biosynthesis was enriched in mpkCCD cells (Supplemental Table 5). Cluster analysis of 250 proteins with the largest standard deviations under three conditions showed six distinctive clusters (Supplemental Figure 8, Supplemental Table 6), indicating that dDAVP and AngII can have similar—or independent—effects on a subset of proteins in mpkDCT or mpkCCD cells.

Identification of DCT- and CCD-Selective Proteins *In Vivo*

To confirm that our data could be translated to the *in vivo* situation, we initially performed immunohistochemistry (IHC) on mouse kidney tissue to localize selective proteins. Double labeling with antibodies against NCC or AQP2 was used to confirm localization to DCT or CCD cells, respectively. As observed in mpkCCD cells, COP9 Signalosome Subunit 6 was highly expressed in CD cells *in vivo*, where it was localized

predominantly to the basolateral membrane of principal cells (Figure 2A). Similarly, compared with the DCT, the E3 ubiquitin ligase CHIP was highly expressed in the CD, where it partially colocalized with AQP2 (Figure 2A, Supplemental Figure 9). Matching the data from mpkDCT cells, the deubiquitylase USP32 was only identified in DCT cells, where it localized to both basolateral and apical membrane domains, with some degree of colocalization with NCC. Similarly, F-Box Protein 2 (FBXO2), was specific for DCT cells, where it colocalized with NCC at the apical plasma membrane. A similar distribution of FBXO2 (Supplemental Figure 10) and CHIP (Supplemental Figure 11) was observed in human kidney tissue. Because technical issues prevented analysis of the majority of commercial antibodies using formaldehyde-fixed, paraffin-embedded tissue or cryosections, we subjected purified DCT cells isolated by FACS from mice with selective green fluorescent protein expression in the DCT to Western blotting. The mpkDCT-enriched proteins FBXO2, SMAD4, SIX4, and FBXO29 were all abundant in isolated DCT cells (Figure 2B). In contrast, the mpkCCD-enriched proteins NRK1, USP4, COP9 Signalosome Subunit 6, and CHIP were not readily detected in isolated DCT cells.

Regulation of CHIP by AVP and Interaction of AQP2 and CHIP in mpkCCD Cells

The differential proteomics approach determined that the E3 ubiquitin ligase CHIP was highly enriched in cultured mpkCCD cells. Immunoblotting of homogenates isolated from different kidney zones (Supplemental Figure 12) confirmed the IHC results, namely that *in vivo* CHIP is expressed throughout the kidney. CHIP abundance was significantly decreased after long-term dDAVP exposure in mpkCCD cells (Supplemental Figure 13A) and mouse kidney (Supplemental Figure 13B).

CHIP binds to the molecular chaperones Hsc70/Hsp70¹⁵ and can alter the turnover of bound clients. Because AQP2 interacts with Hsc70/Hsp70^{16,17} and CHIP is also expressed in CD principal cells, we hypothesized that CHIP regulates AQP2. In mpkCCD14 cell lysates, AQP2, CHIP, Hsc70, and Hsp70 could be detected in samples coimmunoprecipitated using an AQP2-specific antibody (Figure 3A). Similarly, we could identify AQP2 in samples immunoprecipitated using Hsc70 or Hsp70. Technical issues and antibody crossreactivity prevented clear identification of AQP2 in samples immunoprecipitated from mpkCCD cells using a CHIP antibody.

Stable Knockdown of CHIP in mpkCCD Cells Alters AQP2 Protein Abundance and $t_{1/2}$

To examine the role of CHIP in regulation of AQP2, stable knockdown of CHIP in mpkCCD cells using various shRNA constructs was undertaken. Several independent cell populations (A1-A6delCHIP) showed significant reductions in CHIP mRNA by quantitative RT-PCR relative to scrambled shRNA control cells (Supplemental Figure 14A). Significant reductions in CHIP protein were detected in the A1-A6delCHIP

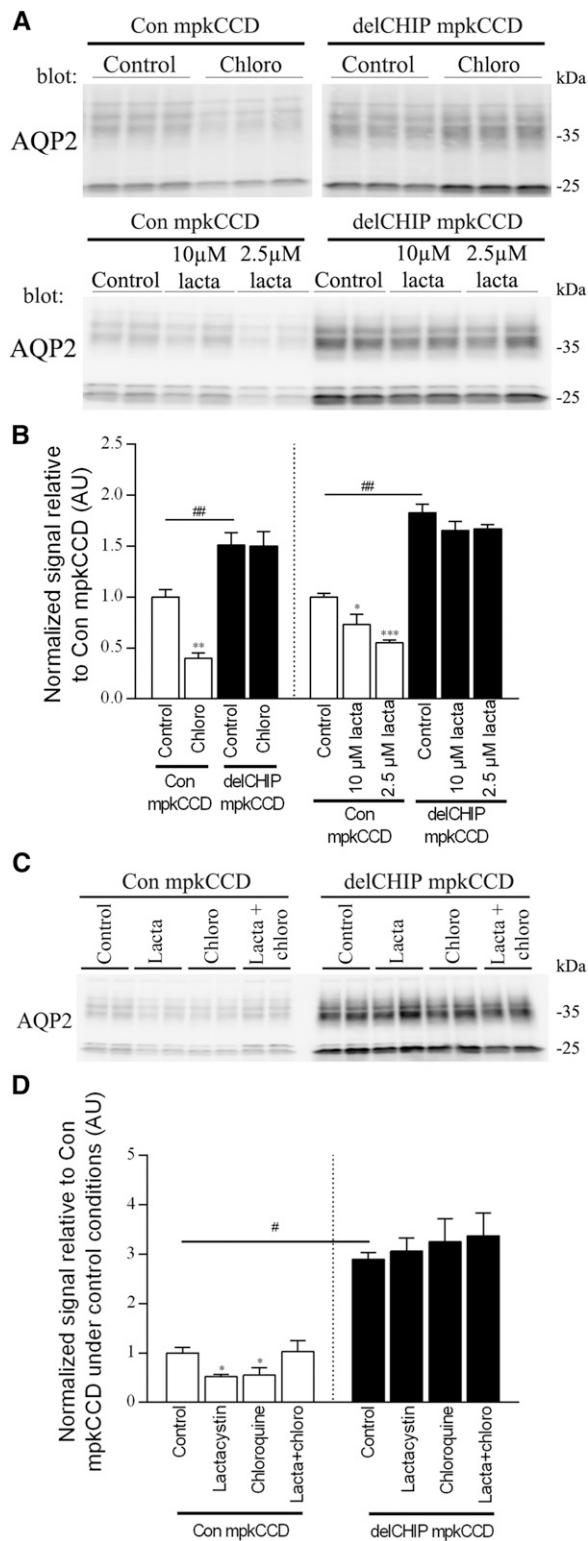


Figure 5. CHIP plays a role in both lysosomal and proteasomal degradation of AQP2. (A) Representative AQP2 immunoblot from cells treated with the lysosomal inhibitor chloroquine (chloro) or the proteasomal inhibitor lactacystin (lacta) for 20 hours. In con mpkCCD cells, AQP2 degradation can occur in the presence of lysosomal or proteasomal inhibition, but this response is absent

lines by Western blotting, which correlated with increased AQP2 levels (Supplemental Figure 14B). One line (termed A4delCHIP) was used for subsequent studies (Supplemental Figure 14C). A consistent reduction in CHIP levels that corresponded with increased AQP2 levels was observed in total protein homogenates from A4delCHIP cells relative to control mpkCCD cells at various cell passage numbers (Figure 3, B and C). Cycloheximide studies (Figure 3D) showed that the increased AQP2 abundance was, at least in part, due to significantly increased AQP2 protein stability and reduced degradation, with the calculated AQP2 protein $t_{1/2}$ in control mpkCCD cells 1.8 hours (95% confidence interval, 1.59 to 1.97) compared with 2.7 hours (95% confidence interval, 2.24 to 2.88) in A4delCHIP cells (Figure 3E).

Inhibition of Hsp90 causes a shift from protein folding to protein degradation *via* CHIP.¹⁸ Supporting a role for CHIP-mediated AQP2 degradation, in control mpkCCD cells treated with the Hsp90 inhibitor 17-*N*-allylamino-17-demethoxygeldanamycin (17-AAG), Hsp70 levels were significantly increased (a key biomarker for the inhibition of Hsp90), and CHIP levels remained constant; however, AQP2 levels were significantly decreased (Figure 4). Despite significantly increased Hsp70 levels in 17-AAG-treated A4delCHIP cells, AQP2 levels remained constant. Furthermore, AQP2 levels were greatly reduced in control mpkCCD cells treated with the Hsp70 activator 2-[[3-Ethyl-5-(3-methyl-2(3H)-benzothiazolylidene)-4-oxo-2-thiazolidinylidene]methyl]-1-methyl-pyridinium chloride (Supplemental Figure 15), supporting a role of Hsp70 in modulating AQP2 expression.

To examine the degradation pathway of AQP2 and the role of CHIP, the lysosomal inhibitor chloroquine and the proteasomal inhibitor lactacystin were used to inhibit the native degradation of AQP2 that occurs in mpkCCD cells after dDAVP removal. In control mpkCCD cells treated with chloroquine or lactacystin (Figure 5, A and B), AQP2 levels were significantly reduced relative to nontreated cells. However, when control mpkCCD cells were treated using chloroquine and lactacystin in combination, AQP2 levels were not significantly altered (Figure 5, C and D). In contrast, under similar conditions, chloroquine or lactacystin had no significant effect on AQP2 levels in A4delCHIP cells (Figure 5,

in A4delCHIP cells. Samples are on the same immunoblot with the same exposure time, and the break is for illustration purposes only. (B) Summary of chloro and lacta data from three independent experiments per treatment. (C) Representative AQP2 immunoblot from cells treated with chloro, lacta, and chloro plus lacta combined. AQP2 levels were not significantly altered when control mpkCCD cells were treated using chloro and lacta in combination. Chloro or lacta alone had no significant effect on AQP2 levels in A4delCHIP cells. (D) Summary of chloro, lacta, and chloro plus lacta combined data from three independent experiments per treatment. Asterisks indicate significance relative to control conditions within an individual cell line; hashtags indicate significance between cell lines. *0.01 < P < 0.05; **0.001 < P < 0.01; *** P < 0.001; #0.01 < P < 0.05; ##0.001 < P < 0.01.

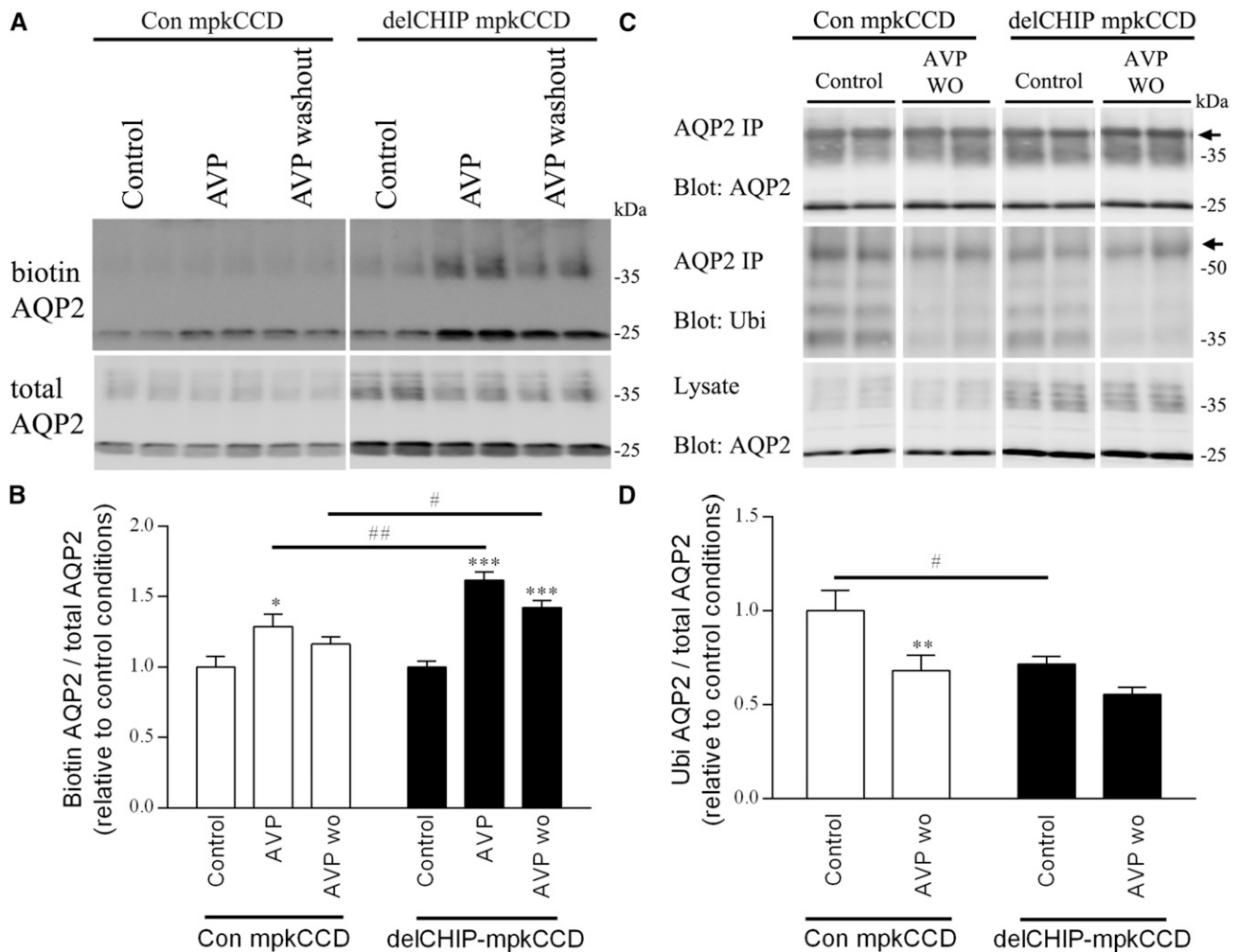


Figure 6. Stable knockdown of CHIP in mpkCCD cells alters AQP2 membrane targeting and ubiquitylation. (A) Representative immunoblots of apically biotinylated AQP2 in control or A4delCHIP cells under control, dDAVP (AVP), or dDAVP followed by 20 minutes washout (AVP washout) conditions. Samples are on the same immunoblot with the same exposure time, and the break is for illustration purposes only. (B) Summary of biotinylation data from five independent experiments. (C) Representative immunoblots of ubiquitylated AQP2 levels in control or A4delCHIP cells under control, dDAVP (AVP), or dDAVP followed by 20 minutes washout (AVP washout) conditions. Samples are on the same immunoblot with the same exposure time, and the break is for illustration purposes only. Arrows represent nonspecific IgG bands. (D) Summary of ubiquitylation data from three independent experiments. Asterisks indicate significance relative to control conditions within an individual cell line; hashtags indicate significance for a specific condition between cell lines. * $0.01 < P < 0.05$; ** $0.001 < P < 0.01$; *** $P < 0.001$; # $0.01 < P < 0.05$; ## $0.001 < P < 0.01$.

C and D). These data indicate that AQP2 can be degraded by both lysosomal or proteasomal pathways and that CHIP plays a role in both processes.

Stable Knockdown of CHIP in mpkCCD Cells Alters AQP2 Membrane Targeting and Ubiquitylation

AQP2 is ubiquitylated, which modulates its plasma membrane accumulation and lysosomal/proteasomal degradation.^{19,20} A role for CHIP in these mechanisms was examined in A4delCHIP cells. Relative to control cells, apical plasma membrane AQP2 levels in A4delCHIP cells were significantly greater after dDAVP stimulation and remained higher 20 minutes after dDAVP removal (Figure 6, A and B). Under identical conditions, ubiquitylated AQP2 levels were significantly lower in untreated

A4delCHIP cells but returned to similar levels as control cells 30 minutes after dDAVP washout (Figure 6, C and D).

CHIP Modifies AQP2 *In Vitro*

CHIP has ubiquitin ligase activity.^{21–24} To assess whether CHIP can directly ubiquitylate AQP2, we performed cellfree ubiquitylation assays. In the presence of ubiquitin, CHIP autoubiquitylation and CHIP-mediated ubiquitylation of Hsc70 were readily detectable (Figure 7).²⁵ AQP2 readily forms stable oligomers that are still present after protein reduction (Figure 7); however, in the presence of CHIP and ubiquitin, AQP2 was modified, resulting in high molecular weight smearing typical of polyubiquitylated proteins. This high molecular weight shift did not occur in reactions lacking CHIP or ubiquitin. Interestingly, modification of AQP2 is

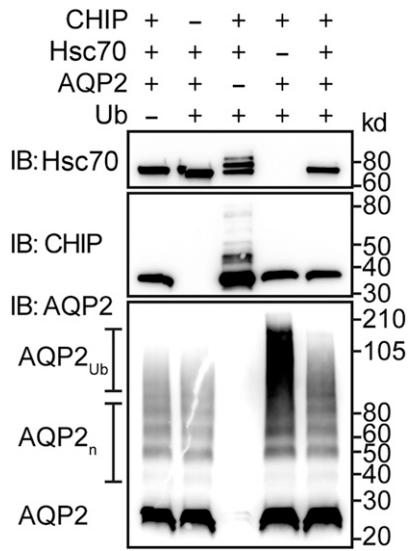


Figure 7. CHIP can ubiquitylate AQP2 *in vitro*. Immunoblot analysis of *in vitro* ubiquitylation reactions in the presence or absence of the various recombinant proteins indicated, including ubiquitin (Ub). The target of antibody used in the immunoblot (IB), molecular mass markers (kilodaltons), and the presence of oligomeric AQP2 (AQP2_n) and polyubiquitylated AQP2 (AQP2_{Ub}) are specified.

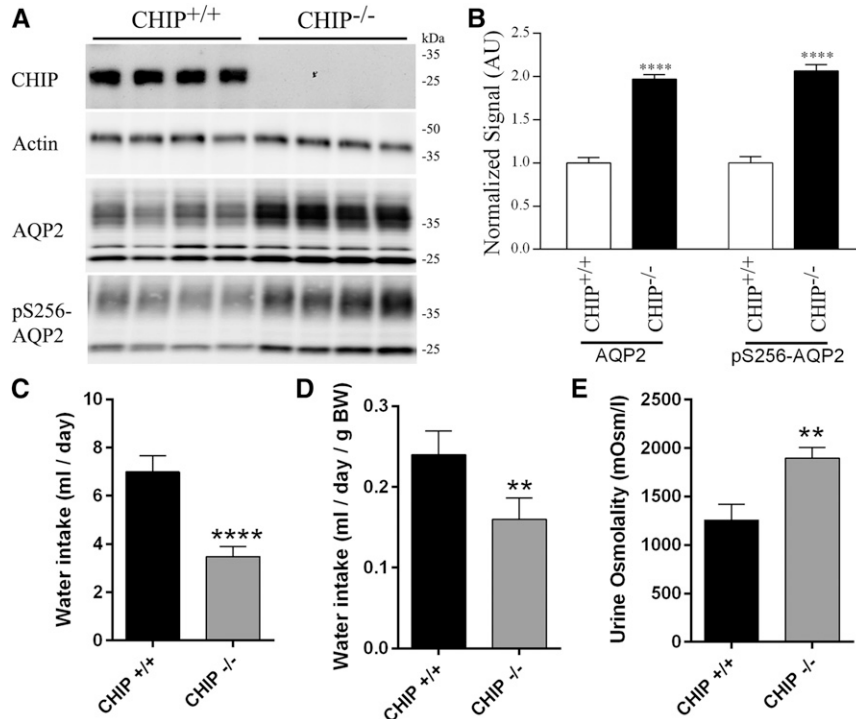


Figure 8. Increased AQP2 levels correlate with altered renal water handling in control (CHIP^{+/+}) and CHIP knockout (CHIP^{-/-}) mice. (A) Representative immunoblots of AQP2 and pS256-AQP2 in CHIP^{+/+} and CHIP^{-/-} mice kidneys. (B) Summary of data from CHIP^{+/+} and CHIP^{-/-} mice, with ten individual mice per genotype. (C) Cumulative data for water intake over a 3-day period. (D) Cumulative data for water intake relative to mouse body weight (BW) over a 3-day period. (E) Cumulative data for urine osmolality over a 3-day period. Asterisks indicate significance between genotypes. **0.001 < P < 0.01; ****P < 0.001.

attenuated in the presence of Hsc70, and the presence of AQP2 prevents both CHIP autoubiquitylation and CHIP-mediated ubiquitylation of Hsc70, suggesting that CHIP can ubiquitylate AQP2 *in vitro*; this interaction may be modified in the presence of Hsc70, altering protein triage.

Increased AQP2 Levels in CHIP Gene-Modified Mice

CHIP was undetectable in CHIP knockout mice (CHIP^{-/-}) (Figure 8A). AQP2 and pS256-AQP2 (a phosphorylation site important for AQP2 trafficking²⁶) levels in kidneys from CHIP^{-/-} mice were significantly greater than those in controls (CHIP^{+/+}) (Figure 8B). pS256-AQP2 levels were not increased in CHIP^{-/-} mice when normalized to total AQP2 levels (Supplemental Figure 16). The increase in total AQP2 was qualitatively confirmed in all regions of the kidney using IHC (Supplemental Figure 17). Similarly, in kidneys from novel mice with a CHIP Thr247Met mutation that results in loss of CHIP ubiquitin ligase activity (CHIP^{M247/M247}), AQP2 and pS256-AQP2 levels were significantly greater than those in control mice (CHIP^{T247/T247}) (Figure 9, A and B). In this model, CHIP levels are also significantly lower (Figure 8, C and D), potentially reflecting the shorter *t*_{1/2} of the mutated CHIP protein.^{27,28} Because of technical difficulties, immunoprecipitating AQP2 from mouse kidney, and detecting ubiquitylated AQP2 with antiubiquitin antibodies, the levels of ubiquitylated AQP2 *in vivo* in the two mouse models could not be determined.

Altered Renal Water Handling in CHIP^{-/-} and CHIP^{M247/M247} Mice

On 3 successive days, CHIP^{-/-} mice had decreased fluid intake (Supplemental Figure 18A), with cumulative fluid intake approximately 2.5-fold less than that of controls (Figure 8, C and D). The osmolality of spontaneously voided urine from CHIP^{-/-} mice was significantly higher on each recorded day (Supplemental Figure 18B), with average urine osmolality in CHIP^{-/-} mice 1.5-fold greater than that of controls (Figure 8E). The higher urine osmolality in CHIP^{-/-} mice relative to controls correlated with significantly greater urine sodium, potassium, chloride, and urea concentrations (Table 1). However, when urinary electrolyte concentrations were normalized to creatinine, no significant differences were observed between the genotypes (Table 1). The CHIP^{M247/M247} mice showed very similar baseline urine electrolyte profiles to the CHIP^{-/-} mice (Table 1), with cumulative fluid intake in CHIP^{M247/M247} mice significantly lower and urine osmolality significantly higher than controls (Figure 9, Supplemental Figure 18, C and D). The baseline serum electrolyte

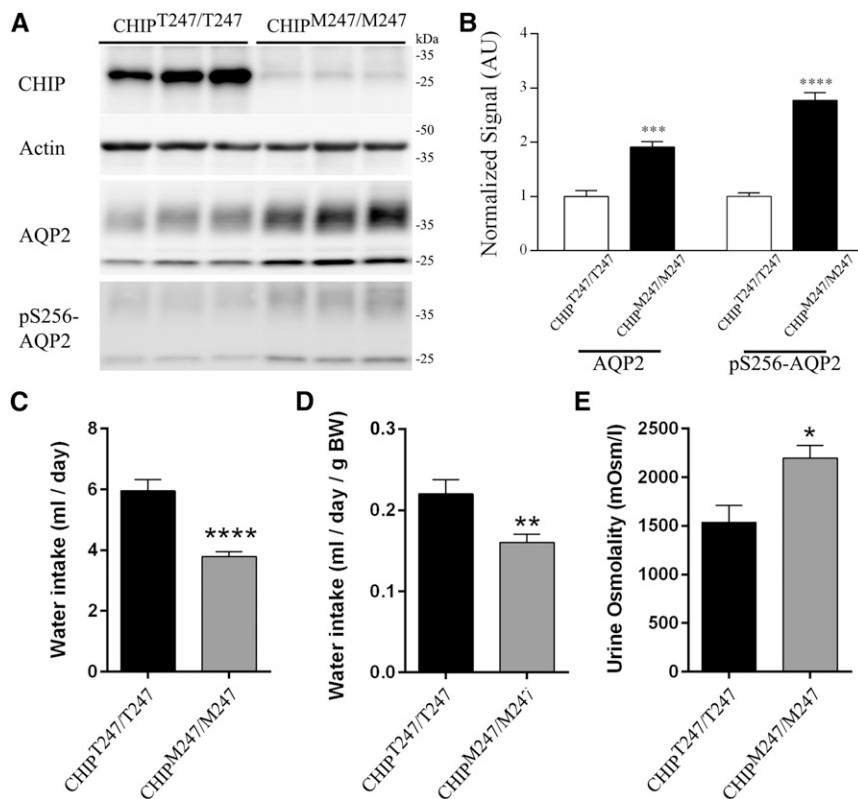


Figure 9. Increased AQP2 levels correlate with altered renal water handling in control (CHIP^{T247/T247}) and CHIP gene-modified (CHIP^{M247/M247}) mice. (A) Representative immunoblots of AQP2 and pS256-AQP2 in CHIP^{T247/T247} and CHIP^{M247/M247} mice kidneys. (B) Summary of data from CHIP^{T247/T247} and CHIP^{M247/M247} mice, with six individual mice per genotype. (C) Cumulative data for water intake over a 3-day period. (D) Cumulative data for water intake relative to mouse body weight (BW) over a 3-day period. (E) Cumulative data for urine osmolality over a 3-day period. Asterisks indicate significance between genotypes. *0.01 < P < 0.05; **0.001 < P < 0.01; ***P < 0.001; ****P < 0.001.

profiles of CHIP^{-/-}, CHIP^{M247/M247}, and relevant control mice were unremarkable, with no significant differences in any of the measured parameters (Table 1).

Expression of Sodium Transporters and AQP2

To examine whether the antidiuresis observed in the CHIP gene-modified mice could be explained by alterations in other transport proteins important for urinary concentration and/or proteins regulated by the AVP signaling pathway,²⁹ we profiled the abundance of other major sodium transporters and AQP2 in kidneys from CHIP^{-/-}, CHIP^{M247/M247}, and relevant control mice. No significant differences in abundance between the gene-modified mice and relevant controls were observed for any of the examined proteins (Figure 10).

DISCUSSION

Epithelial cells of the DCT and CCD both segregate and integrate the transport of water, solutes, and ions to maintain systemic levels of these substances and thus, body homeostasis. Despite this critical role, very little was known about which proteins play a regulatory role in DCT and CCD cells and how these cell types can be differentially regulated by similar physiologic stimuli. The major goal here was to use a systems biology approach to identify novel and unique regulatory proteins important for modulation of DCT and CCD function.

Table 1. Baseline urine and serum electrolyte profile of CHIP^{-/-} and CHIP^{M247/M247} mice

Parameter	CHIP ^{+/+}	CHIP ^{-/-}	P Value	CHIP ^{T247/T247}	CHIP ^{M247/M247}	P Value
Plasma						
Osmolality, mOsm/kg H ₂ O	374±8	370±4	ns	375±6	369±3	ns
Na ⁺ , mmol/L	147±0.5	146±0.5	ns	147±1	145±0.5	ns
K ⁺ , mmol/L	4.92±0.17	4.76±0.39	ns	4.85±0.26	4.65±0.29	ns
Cl ⁻ , mmol/L	114±1	114±0.5	ns	114±2	113±1	ns
Urea, mmol/L	10.6±0.6	10.4±0.4	ns	8.6±0.3	8.0±0.5	ns
Urine						
Na ⁺ , mmol/L	70±11	97±5	<0.05	67±7	93±8	<0.05
Na ⁺ -to-creatinine ratio	24±2	28±3	ns	27±4	27±3	ns
K ⁺ , mmol/L	94±11	141±8	<0.01	110±9	145±9	<0.05
K ⁺ -to-creatinine ratio	34±4	38±3	ns	38±2	39±2	ns
Cl ⁻ , mmol/L	145±26	202±5	<0.05	154±14	194±17	ns
Cl ⁻ -to-creatinine ratio	50±5	55±4	ns	56±6	54±5	ns
Urea, mmol/L	990±91	1349±112	<0.05	960±60	1313±79	<0.01
Urea-to-creatinine ratio	354±31	354±18	ns	347±24	351±19	ns
Creatinine, mmol/L	2.8±0.2	3.8±0.3	<0.01	2.9±0.3	3.8±0.3	<0.05

Na⁺, Sodium; K⁺, Potassium; Cl⁻, Chloride.

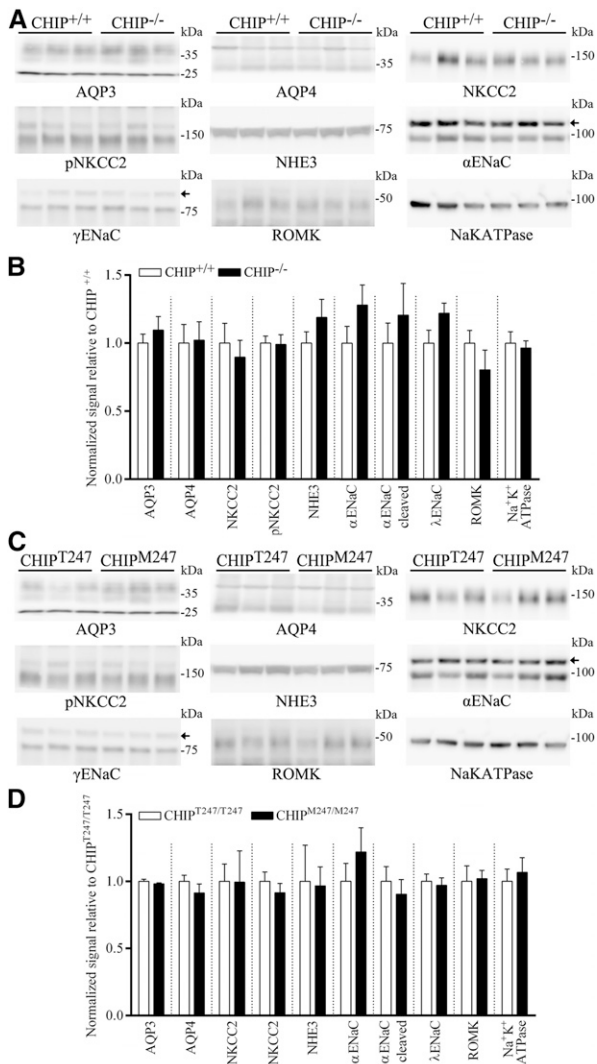


Figure 10. Abundances of other major sodium transporters and AQP2 in kidneys from $CHIP^{-/-}$, $CHIP^{M247/M247}$, and relevant control mice. (A) Representative immunoblots of AQP3, AQP4, NKCC2, pNKCC2, NHE3, α -epithelial sodium channel (α ENaC), γ ENaC, ROMK, and Na-K-ATPase in $CHIP^{+/+}$ and $CHIP^{-/-}$ mice kidneys. Small arrows indicate nonspecific bands. (B) Summary of data from $CHIP^{+/+}$ and $CHIP^{-/-}$ mice, with ten individual mice per genotype. (C) Representative immunoblots of AQP3, AQP4, NKCC2, pNKCC2, NHE3, α ENaC, β ENaC, ROMK, and Na-K-ATPase in $CHIP^{T247/T247}$ and $CHIP^{M247/M247}$ mice kidneys. (D) Summary of data from $CHIP^{T247/T247}$ and $CHIP^{M247/M247}$ mice, with six individual mice per genotype.

mpkCCD and mpkDCT cells are excellent models of the CCD and DCT.^{2,4-6} Our SILAC-based large-scale quantitative LC-MS/MS³⁰ allowed exceptional quantitative comparisons of their proteomes and has generated a large unbiased database that will provide a solid foundation for detailed targeted investigations into the roles of various proteins for regulating various homeostatic mechanisms unique to DCT and CCD cells.

Our proteomics data allowed us to generate and test the novel hypothesis that the CCD-enriched cochaperone and E3

ubiquitin ligase CHIP would play a role in modulating the function of AQP2. It is well established that, in the endoplasmic reticulum, the chaperone proteins Hsp90 and Hsp70 play essential roles in maintaining the balance between protein folding and ubiquitin-dependent proteasomal degradation.³¹ If Hsp70-bound proteins are bound to the cochaperone Hop, this facilitates their association with the Hsp90 complex, promoting folding of the client protein. However, Hsp70-bound proteins associating with CHIP are targeted to endoplasmic reticulum-associated degradation *via* the ubiquitin proteasome system.³²⁻³⁴ The association of AQP2, CHIP, and Hsp70 in a protein complex plus the greater abundance of AQP2 in mpkCCD cells with stable knockdown of CHIP or in $CHIP$ gene-modified mice suggest that AQP2 is subject to similar quality control (QC) mechanisms. Therefore, in the absence of CHIP, there is a shift in balance toward AQP2 protein folding rather than degradation. Support for the involvement of this pathway for regulation of AQP2 includes the continued degradation of AQP2 in mpkCCD cells during lysosomal inhibition (but not combined lysosomal/proteasomal inhibition), the increased AQP2 protein $t_{1/2}$ in CHIP-deficient cells, and the fact that inhibition of Hsp90 in control but not CHIP-deficient mpkCCD cells decreased AQP2 abundance.

Coimmunoprecipitation indicated that, in addition to Hsp70, AQP2:CHIP may also form a complex with Hsc70. AQP2:Hsc70 complexes have been identified,^{16,17} and the role of this interaction has focused on AQP2 endocytosis. Because CHIP plays a role in plasma membrane QC (peripheral QC),³⁵ it may also play a role in modulating AQP2 endocytosis (Figure 11), similar to, for example, unfolded CFTR.³⁶ Such a mechanism is supported by (1) partial colocalization of CHIP and AQP2 in the apical plasma membrane domain of CD principal cells, (2) reduced AQP2 ubiquitylation in CHIP-deficient cells, (3) higher abundance of AQP2 in the apical plasma membrane in response to AVP in CHIP-deficient cells, and (4) greater abundance of AQP2 in the plasma membrane of CHIP-deficient cells after AVP removal. However, one caveat to this mechanism is that, in the presence of Hsc70, CHIP-mediated polyubiquitylation of AQP2 *in vitro* was reduced. This could indicate that an Hsc70:AQP2 complex limits CHIP-mediated ubiquitylation or that peripheral QC of AQP2 involves an additional as yet unidentified E3 ligase.³⁵ A variety of other E3 ubiquitin ligases have been identified in CD cells that may be important for modulation of AQP2 function.^{37,38}

The physiologic importance of CHIP for modulating AQP2 *in vivo* was shown in two gene-modified mice models, which had increased AQP2 levels, decreased fluid intake, and greater urine osmolality relative to controls. The animals do not seem to have “positive water balance,” because plasma electrolyte levels in the two models are not significantly different from controls. To some extent, the animals resemble a model of nephrogenic syndrome of inappropriate antidiuresis³⁹ but seem to compensate by drinking less to maintain steady state and normal plasma osmolality/electrolytes. On the basis of these data, pharmaceutical inhibition of CHIP could be a novel approach to treat certain forms of nephrogenic diabetes insipidus and prevent the peripheral QC-mediated internalization of misfolded AQP2 mutants that may

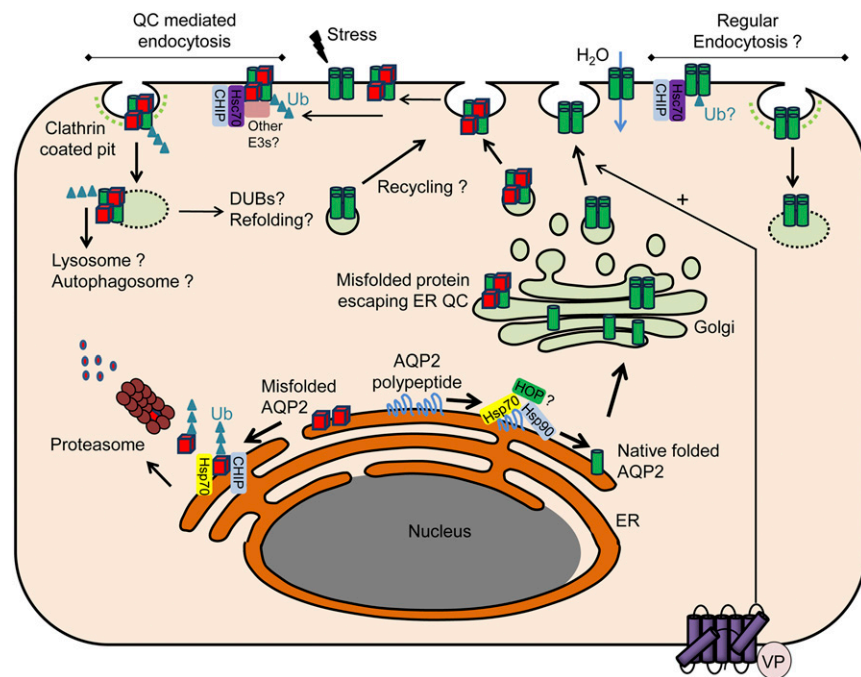


Figure 11. Potential role of CHIP in AQP2 QC and trafficking. In the endoplasmic reticulum (ER) under normal physiologic conditions, AQP2 polypeptide is bound by the chaperone protein Hsp70. The cochaperone Hop facilitates the association with the Hsp90 complex, promoting native folding of AQP2 that traffics to the Golgi apparatus, is organized into tetramers, and stored in transport vesicles. As part of the ER QC, Hsp70-bound AQP2 that is misfolded under normal conditions or after cellular stress associates with CHIP and is targeted to endoplasmic reticulum-associated degradation (ERAD) via the ubiquitin proteasome system. Other ERAD-associated E3 ligases are likely to be involved in ubiquitylation of AQP2. Despite ER QC, a proportion of AQP2 escapes to the Golgi apparatus and is subsequently stored in transport vesicles. Folded and misfolded AQP2 traffics to the plasma membrane (PM) after AVP (VP) stimulation. Because of peripheral QC, ER-misfolded AQP2 or AQP2 misfolded within the PM due to environmental stresses are recognized and bound by Hsc70. Hsc70 associates with CHIP and other E3 ligases promoting AQP2 endocytosis and degradation. Alternatively, internalized AQP2 may be deubiquitylated, refolded, and recycled to the PM. In addition to QC-mediated endocytosis, regular AQP2 endocytosis may involve Hsc70/CHIP. A number of the collecting duct-specific E3 ligases and deubiquitylases (DUBs) identified may play important roles in these processes. Ub, ubiquitin.

reach the plasma membrane but are functional.⁴⁰ Such an approach to control the peripheral QC therapeutically was proposed for misfolded CFTR.⁴¹ Alternatively, activation of CHIP-mediated protein QC should substantially reduce the enhanced levels of AQP2 observed in various diseases with water retention (e.g., congestive heart failure or liver cirrhosis).⁴⁰

CONCISE METHODS

Extensive methods are included as Supplemental Material.

SILAC Labeling, High-pH Reversed Phase Fractionation, Nanoliquid Chromatography and Mass Spectrometry, Mass Spectrometry Data Analyses, and Bioinformatics

Extensive details are in Supplemental Material. The mass spectrometry data have been deposited to the ProteomeXchange Consortium

via the PRIDE⁴² partner repository with the dataset identifier PXD005454.

Isolation of Enhanced Green Fluorescent Protein-Expressing Mouse DCT Cells

All animal protocols were performed in accordance with licenses for the use of experimental animals issued by the Danish Ministry of Justice. Extensive details are in Supplemental Material. Enhanced green fluorescent protein (EGFP) purity changed from 4% before sorting to 94% after sorting in the EGFP-positive sample and 0% in the EGFP-negative sample.

Antibodies

For Western blotting, the antibodies used, the supplier, and the predicted molecular weight of the target protein are detailed in Supplemental Table 7.

Fluorescent IHC and Confocal Microscopy Analyses

Mouse kidney tissue was processed and labeled as previously described.⁴³

Generation of mpkCCD Cells with Stable CHIP Knockdown

Generation of mpkCCD cells with stable CHIP knockdown was performed as previously described⁴⁴ using MISSION lentiviral transduction particles against CHIP (nos. 8527, 8528, 8530, 280520, and 280575) and corresponding control particles (SHC002V) from Sigma-Aldrich.

Real-Time Quantitative PCR

Real-time quantitative PCR was performed as previously described.⁴⁴

mpkCCD14 Culture and Experimental Conditions for CHIP Analyses

mpkCCD14 cells were cultured on semipermeable supports as previously described.⁴⁵ For acute dDAVP stimulation, cells were washed twice in pure media and reincubated in pure media for 3 hours before being restimulated with dDAVP (1 nM) from the basolateral side for 20 minutes at 37°C. In dDAVP washout experiments, cells were subsequently washed twice in pure media and reincubated for 30 minutes at 37°C before sample preparation. For 17-AAG studies, indicated cells were incubated with 2 μ M 17-AAG for 16 hours before harvest. For Hsp70 activation studies, indicated cells were incubated with 5 μ M 2-[[3-Ethyl-5-(3-methyl-2(3H)-benzothiazolylidene)-4-oxo-2-thiazolidinylidene]methyl]-1-methyl-pyridinium chloride (Sigma-Aldrich) for 16 hours in the presence of dDAVP before harvest. For proteasomal and lysosomal inhibition experiments, after 72 hours of dDAVP treatment, cells were washed twice in pure media and reincubated in pure media for 8 hours

in the presence of 10 μ M lactacystin, 150 μ M chloroquine, or both as indicated. For cycloheximide chase studies, cells were incubated for various time points at 37°C and 5% CO₂ in 50 μ M cycloheximide.

Surface Biotinylation of mpkCCD14 Cells

Apical plasma membrane proteins were labeled with EZ-link hydrazide-biotin (Pierce) as previously described.⁴⁵

Immunoprecipitation Using mpkCCD14 Cells

Immunoprecipitation was performed as previously described.⁴⁶

CHIP-Deficient Mice

Mice lacking CHIP expression (*Stub1* targeted knockout, gene identification 56424) B6;129-*Stub1*^{tm1Cpat}/Mmnc (RRID:MMRRC_037422-UNC) on a mixed background of 129S/SvEv and C57BL/6 were previously reported.⁴⁷ For this line, knockout mice are delineated (CHIP^{-/-}), and control animals are age- and sex-matched wild-type littermate controls (referred to as CHIP^{+/+}).

Generation of CHIP (Stub1 Gene) T247M Mutant Mice

Extensive details of guide RNA cloning, guide RNA *in vitro* transcription, guide RNA activity test, *in vitro* cleavage assays, mouse production, genotyping, and off-target analysis are in Supplemental Material. For this line, knock-in mice are delineated (CHIP^{M247/M247}), and control animals are age- and sex-matched wild-type littermate controls (referred to as CHIP^{T247/T247}).

Water Intake and Urine Collection in CHIP^{-/-} and CHIP^{M247/M247} Mice

All animal use was approved by the Institutional Animal Care and Use Committee at the University of North Carolina at Chapel Hill under protocol 16–066. Extensive details are provided in Supplemental Material.

In Vitro Ubiquitylation Reactions

In vitro ubiquitylation reactions were performed as previously described.²³

Statistical Analyses

For Western blotting and mouse physiologic recordings, data are expressed as mean \pm SEM. For two groups, data meeting the statistical assumptions of normality were assessed using an unpaired *t* test. Comparisons of more than two groups were performed using either a one-way ANOVA or a two-way repeated measures ANOVA followed by the Student–Newman–Keuls or the Tukey multiple comparison test, respectively. Significance was considered at $P < 0.05$.

ACKNOWLEDGMENTS

We would like to acknowledge the technical assistance of Inger-Merete Paulsen, Helle Høyer, Tina Drejer, Ahmed Abduljabar, and Christian Westberg. We also thank John Blake Belcher, Sabrina Madrigal, and Anna Elizabeth Robertson for their help with animal studies. The Animal Models Core directed by Dale Cowley at The University of North Carolina at Chapel Hill is thanked for assistance.

Q.W. is supported by European Union Horizon 2020 Marie Skłodowska-Curie Individual Fellowship project 705682, Danish Medical Research Council grant 6110-00118B, and Lundbeck Foundation grant R192-2015-804. M.L.A.K. is supported by Danish Medical Research Council grant 1333-00279. Funding is provided by National Institutes of Health grant R37 HL065619 (to C.P. and J.C.S.). Funding is also provided by the Novo Nordisk Foundation (R.A.F.), the Lundbeck Foundation (R.A.F.), and the Danish Medical Research Council (R.A.F.).

All authors approved the final version of the manuscript and agree to be accountable for all aspects of the work in ensuring that questions related to the accuracy or integrity of any part of the work are appropriately investigated and resolved. All persons designated as authors qualify for authorship, and all those who qualify for authorship are listed.

DISCLOSURES

None.

REFERENCES

1. Skorecki K, Chertow GM, Marsden PA, Taal MW, Yu ASL, Luyckx V: *Brenner and Rector's the Kidney*, Philadelphia, Elsevier, 2015
2. Subramanya AR, Ellison DH: Distal convoluted tubule. *Clin J Am Soc Nephrol* 9: 2147–2163, 2014
3. Kortenoeven ML, Fenton RA: Renal aquaporins and water balance disorders. *Biochim Biophys Acta* 1840: 1533–1549, 2014
4. Kortenoeven ML, Pedersen NB, Rosenbaek LL, Fenton RA: Vasopressin regulation of sodium transport in the distal nephron and collecting duct. *Am J Physiol Renal Physiol* 309: F280–F299, 2015
5. Giebisch G: Hormonal control of distal nephron function. *Klin Wochenschr* 63: 877–885, 1985
6. Pearce D, Soundararajan R, Trimpert C, Kashlan OB, Deen PM, Kohan DE: Collecting duct principal cell transport processes and their regulation. *Clin J Am Soc Nephrol* 10: 135–146, 2015
7. Hennings JC, Andrini O, Picard N, Paulais M, Huebner AK, Cayuqueo IK, Bignon Y, Keck M, Cornière N, Böhm D, Jentsch TJ, Chambrey R, Teulon J, Hübner CA, Eladari D: The ClC-K2 chloride channel is critical for salt handling in the distal nephron. *J Am Soc Nephrol* 28: 209–217, 2017
8. Valles P, Wysocki J, Batlle D: Angiotensin II and renal tubular ion transport. *Sci World J* 5: 680–690, 2005
9. Yu MJ, Miller RL, Uawithya P, Rinschen MM, Khositseth S, Braucht DW, Chou CL, Pisitkun T, Nelson RD, Knepper MA: Systems-level analysis of cell-specific AQP2 gene expression in renal collecting duct. *Proc Natl Acad Sci U S A* 106: 2441–2446, 2009
10. Loo CS, Chen CW, Wang PJ, Chen PY, Lin SY, Khoo KH, Fenton RA, Knepper MA, Yu MJ: Quantitative apical membrane proteomics reveals vasopressin-induced actin dynamics in collecting duct cells. *Proc Natl Acad Sci U S A* 110: 17119–17124, 2013
11. Rajagopal M, Kathpalia PP, Widdicombe JH, Pao AC: Differential effects of extracellular ATP on chloride transport in cortical collecting duct cells. *Am J Physiol Renal Physiol* 303: F483–F491, 2012
12. Cheng L, Wu Q, Kortenoeven ML, Pisitkun T, Fenton RA: A systems level analysis of vasopressin-mediated signaling networks in kidney distal convoluted tubule cells. *Sci Rep* 5: 12829, 2015
13. Gao T, Liu Z, Wang Y, Cheng H, Yang Q, Guo A, Ren J, Xue Y: UUCD: A family-based database of ubiquitin and ubiquitin-like conjugation. *Nucleic Acids Res* 41: D445–D451, 2013

14. Zhang HM, Chen H, Liu W, Liu H, Gong J, Wang H, Guo AY: AnimalTFDB: A comprehensive animal transcription factor database. *Nucleic Acids Res* 40: D144–D149, 2012
15. McDonough H, Patterson C: CHIP: A link between the chaperone and proteasome systems. *Cell Stress Chaperones* 8: 303–308, 2003
16. Lu HA, Sun TX, Matsuzaki T, Yi XH, Eswara J, Bouley R, McKee M, Brown D: Heat shock protein 70 interacts with aquaporin-2 and regulates its trafficking. *J Biol Chem* 282: 28721–28732, 2007
17. Moeller HB, Praetorius J, Rützler MR, Fenton RA: Phosphorylation of aquaporin-2 regulates its endocytosis and protein-protein interactions. *Proc Natl Acad Sci U S A* 107: 424–429, 2010
18. Kundrat L, Regan L: Balance between folding and degradation for Hsp90-dependent client proteins: A key role for CHIP. *Biochemistry* 49: 7428–7438, 2010
19. Kamsteeg EJ, Hendriks G, Boone M, Konings IB, Oorschot V, van der Sluijs P, Klumperman J, Deen PM: Short-chain ubiquitination mediates the regulated endocytosis of the aquaporin-2 water channel. *Proc Natl Acad Sci U S A* 103: 18344–18349, 2006
20. Nedvetsky PI, Tabor V, Tamma G, Beulshausen S, Skroblin P, Kirschner A, Mutig K, Boltzen M, Petrucci O, Vossenkämper A, Wiesner B, Bachmann S, Rosenthal W, Klusmann E: Reciprocal regulation of aquaporin-2 abundance and degradation by protein kinase A and p38-MAP kinase. *J Am Soc Nephrol* 21: 1645–1656, 2010
21. Ballinger CA, Connell P, Wu Y, Hu Z, Thompson LJ, Yin LY, Patterson C: Identification of CHIP, a novel tetratricopeptide repeat-containing protein that interacts with heat shock proteins and negatively regulates chaperone functions. *Mol Cell Biol* 19: 4535–4545, 1999
22. Connell P, Ballinger CA, Jiang J, Wu Y, Thompson LJ, Höhfeld J, Patterson C: The co-chaperone CHIP regulates protein triage decisions mediated by heat-shock proteins. *Nat Cell Biol* 3: 93–96, 2001
23. Jiang J, Ballinger CA, Wu Y, Dai Q, Cyr DM, Höhfeld J, Patterson C: CHIP is a U-box-dependent E3 ubiquitin ligase: Identification of Hsc70 as a target for ubiquitylation. *J Biol Chem* 276: 42938–42944, 2001
24. Schisler JC, Rubel CE, Zhang C, Lockyer P, Cyr DM, Patterson C: CHIP protects against cardiac pressure overload through regulation of AMPK. *J Clin Invest* 123: 3588–3599, 2013
25. Shi CH, Schisler JC, Rubel CE, Tan S, Song B, McDonough H, Xu L, Portbury AL, Mao CY, True C, Wang RH, Wang QZ, Sun SL, Seminara SB, Patterson C, Xu YM: Ataxia and hypogonadism caused by the loss of ubiquitin ligase activity of the U box protein CHIP. *Hum Mol Genet* 23: 1013–1024, 2014
26. Moeller HB, Olesen ET, Fenton RA: Regulation of the water channel aquaporin-2 by posttranslational modification. *Am J Physiol Renal Physiol* 300: F1062–F1073, 2011
27. Hayer SN, Deconinck T, Bender B, Smets K, Züchner S, Reich S, Schöls L, Schüle R, De Jonghe P, Baets J, Synofzik M: STUB1/CHIP mutations cause Gordon Holmes syndrome as part of a widespread multisystemic neurodegeneration: Evidence from four novel mutations. *Orphanet J Rare Dis* 12: 31, 2017
28. Heimdal K, Sanchez-Guixé M, Aukrust I, Bollerslev J, Bruland O, Jablonski GE, Erichsen AK, Gude E, Koht JA, Erdal S, Fiskerstrand T, Haukanes BI, Boman H, Bjørkhaug L, Tallaksen CM, Knappskog PM, Johansson S: STUB1 mutations in autosomal recessive ataxias—evidence for mutation-specific clinical heterogeneity. *Orphanet J Rare Dis* 9: 146, 2014
29. Fenton RA, Knepper MA: Mouse models and the urinary concentrating mechanism in the new millennium. *Physiol Rev* 87: 1083–1112, 2007
30. Mann M: Functional and quantitative proteomics using SILAC. *Nat Rev Mol Cell Biol* 7: 952–958, 2006
31. Edkins AL: CHIP: A co-chaperone for degradation by the proteasome. *Subcell Biochem* 78: 219–242, 2015
32. Li P, Kurata Y, Maharani N, Mahati E, Higaki K, Hasegawa A, Shirayoshi Y, Yoshida A, Kondo T, Kurozawa Y, Yamamoto K, Ninomiya H, Hisatome I: E3 ligase CHIP and Hsc70 regulate Kv1.5 protein expression and function in mammalian cells. *J Mol Cell Cardiol* 86: 138–146, 2015
33. Younger JM, Ren HY, Chen L, Fan CY, Fields A, Patterson C, Cyr DM: A foldable CFTRDeltaF508 biogenic intermediate accumulates upon inhibition of the Hsc70-CHIP E3 ubiquitin ligase. *J Cell Biol* 167: 1075–1085, 2004
34. McCaffrey K, Braakman I: Protein quality control at the endoplasmic reticulum. *Essays Biochem* 60: 227–235, 2016
35. Apaja PM, Lukacs GL: Protein homeostasis at the plasma membrane. *Physiology (Bethesda)* 29: 265–277, 2014
36. Okiyoneda T, Barrière H, Bagdány M, Rabeh WM, Du K, Höhfeld J, Young JC, Lukacs GL: Peripheral protein quality control removes unfolded CFTR from the plasma membrane. *Science* 329: 805–810, 2010
37. Medvar B, Raghuram V, Pisitkun T, Sarkar A, Knepper MA: Comprehensive database of human E3 ubiquitin ligases: Application to aquaporin-2 regulation. *Physiol Genomics* 48: 502–512, 2016
38. Lee YJ, Lee JE, Choi HJ, Lim JS, Jung HJ, Baek MC, Frøkiær J, Nielsen S, Kwon TH: E3 ubiquitin-protein ligases in rat kidney collecting duct: Response to vasopressin stimulation and withdrawal. *Am J Physiol Renal Physiol* 301: F883–F896, 2011
39. Feldman BJ, Rosenthal SM, Vargas GA, Fenwick RG, Huang EA, Matsuda-Abedini M, Lustig RH, Mathias RS, Portale AA, Miller WL, Gitelman SE: Nephrogenic syndrome of inappropriate antidiuresis. *N Engl J Med* 352: 1884–1890, 2005
40. Moeller HB, Rittig S, Fenton RA: Nephrogenic diabetes insipidus: Essential insights into the molecular background and potential therapies for treatment. *Endocr Rev* 34: 278–301, 2013
41. Loureiro CA, Matos AM, Dias-Alves Á, Pereira JF, Uliyakina I, Barros P, Amaral MD, Matos P: A molecular switch in the scaffold NHERF1 enables misfolded CFTR to evade the peripheral quality control checkpoint. *Sci Signal* 8: ra48, 2015
42. Vizcaino JA, Csordas A, del-Toro N, Dianas JA, Griss J, Lavidas I, Mayer G, Perez-Riverol Y, Reisinger F, Tement T, Xu QW, Wang R, Hermjakob H: 2016 update of the PRIDE database and its related tools. *Nucleic Acids Res* 44: D447–D456, 2016
43. Moeller HB, Knepper MA, Fenton RA: Serine 269 phosphorylated aquaporin-2 is targeted to the apical membrane of collecting duct principal cells. *Kidney Int* 75: 295–303, 2009
44. Yde J, Keely S, Wu Q, Borg JF, Lajczak N, O'Dwyer A, Dalsgaard P, Fenton RA, Moeller HB: Characterization of AQPs in mouse, rat, and human colon and their selective regulation by bile acids. *Front Nutr* 3: 46, 2016
45. Moeller HB, Slengerik-Hansen J, Aroankins T, Assentoft M, MacAulay N, Moestrup SK, Bhalla V, Fenton RA: Regulation of the water channel aquaporin-2 via 14-3-3 θ and ζ . *J Biol Chem* 291: 2469–2484, 2016
46. Moeller HB, Aroankins TS, Slengerik-Hansen J, Pisitkun T, Fenton RA: Phosphorylation and ubiquitylation are opposing processes that regulate endocytosis of the water channel aquaporin-2. *J Cell Sci* 127: 3174–3183, 2014
47. Dai Q, Zhang C, Wu Y, McDonough H, Whaley RA, Godfrey V, Li HH, Madamanchi N, Xu W, Neckers L, Cyr D, Patterson C: CHIP activates HSF1 and confers protection against apoptosis and cellular stress. *EMBO J* 22: 5446–5458, 2003

This article contains supplemental material online at <http://jasn.asnjournals.org/lookup/suppl/doi:10.1681/ASN.2017050526/-/DCSupplemental>.

Supplemental Information for

CHIP regulates Aquaporin-2 Quality Control and Body Water Homeostasis

Table of Contents

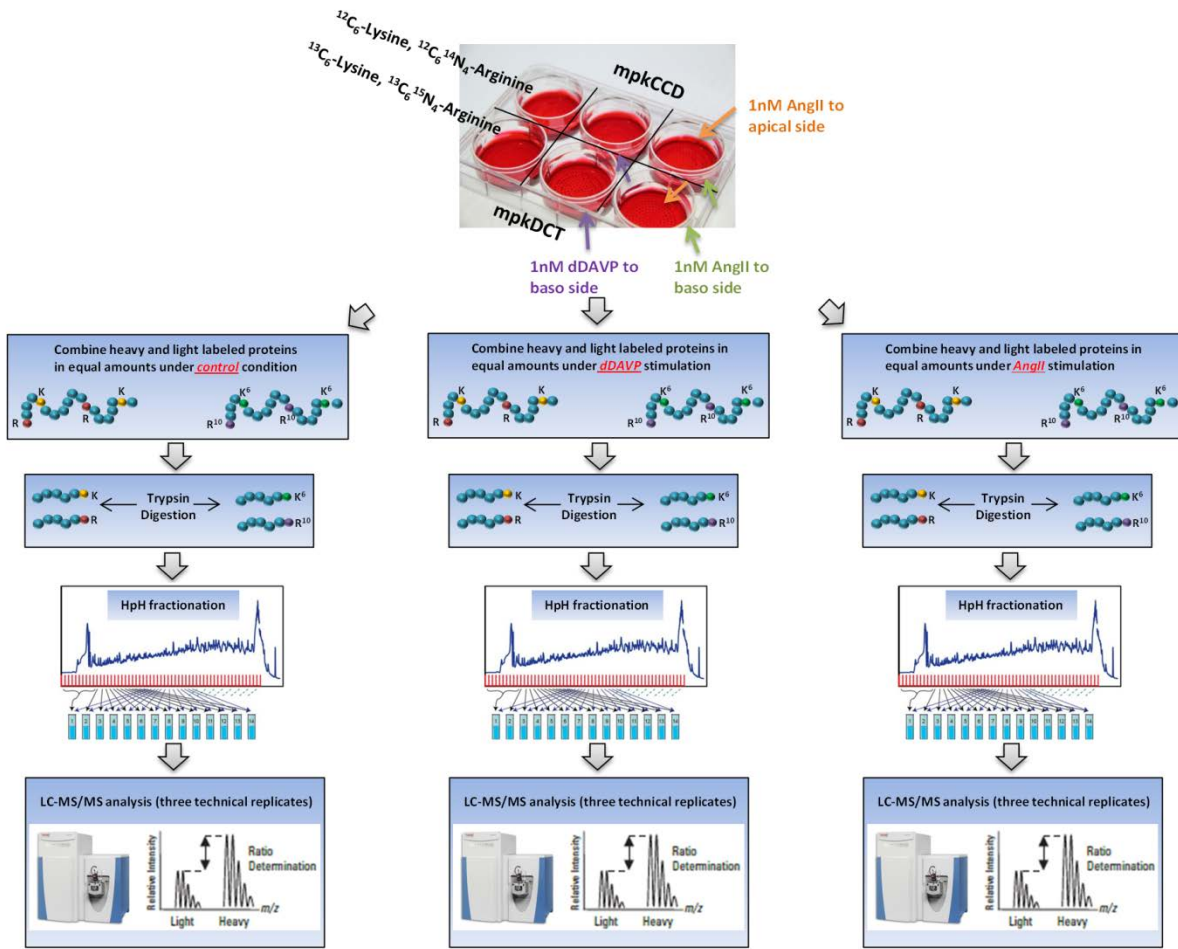
Supplemental Table 7.....Page 2

Supplemental Figures 1-18.....Pages 3-20

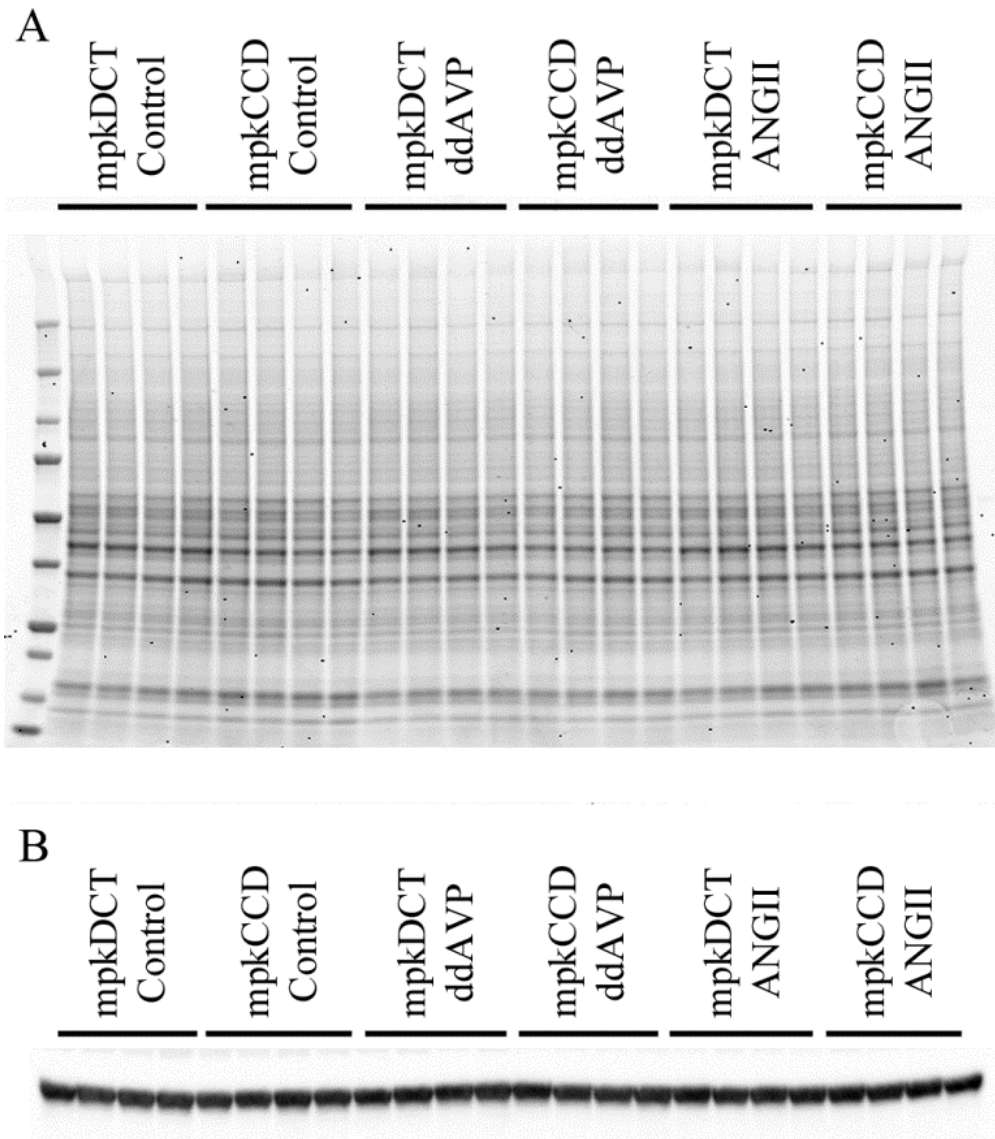
Supplemental Detailed Methods.....Pages 21-34

Supplemental Table 7. Detailed information on Antibodies

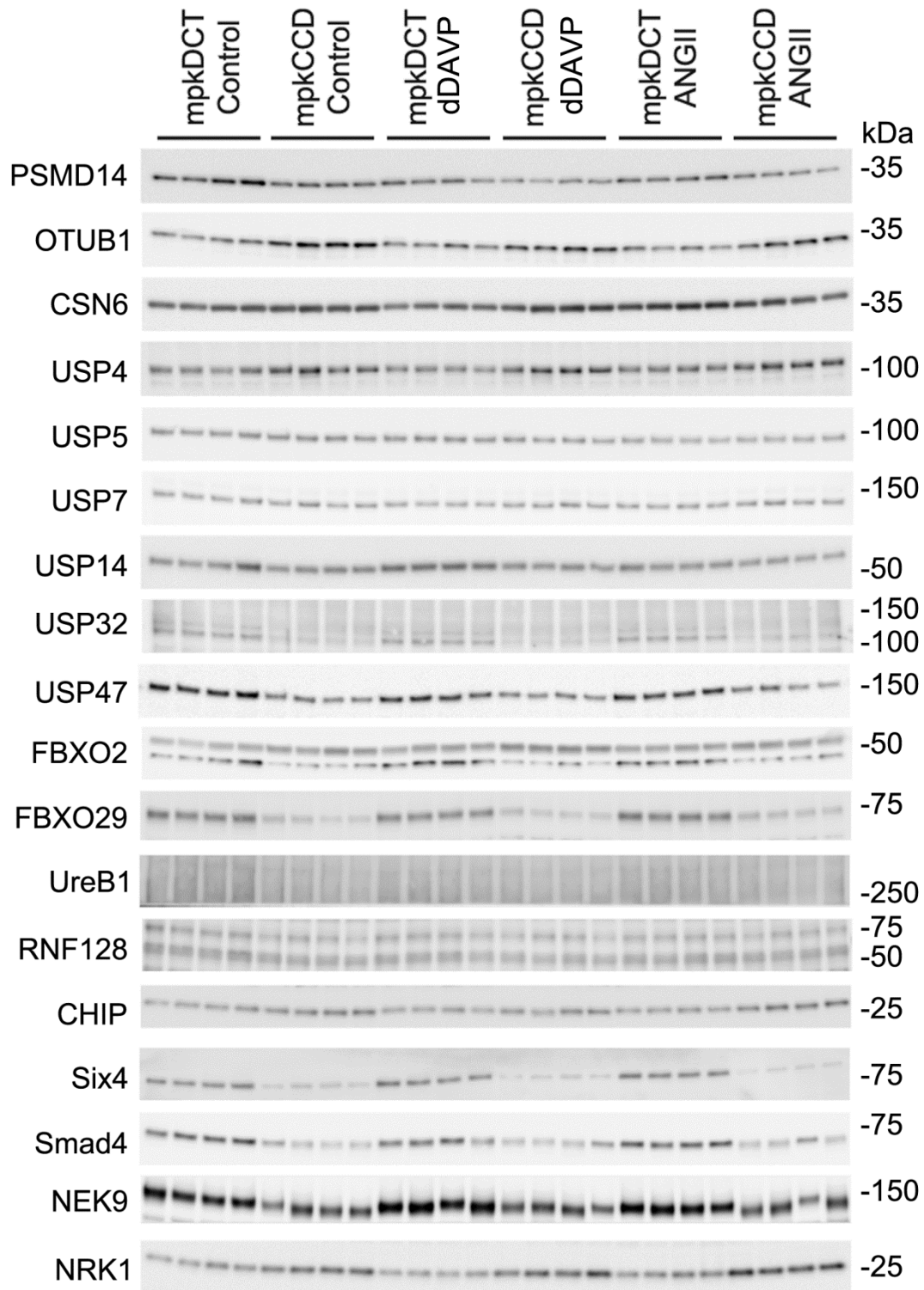
Antibody	Supplier	Cat. No. or Reference	Predicted MW (kDa)
Ubiquitin	Cell Signaling	3936	N/A
PSMD14	Cell Signaling	4197	35
USP14	Cell Signaling	11931	60
USP4	Cell Signaling	2651	110
OTUB1	Abcam	ab82154	31
RNF128	Abcam	ab72533	45-70
CHIP (Stub1)	Abcam	ab134064	35
Proteasome 20S	Abcam	ab3325	30
AQP3	Abcam	ab153694	25 and 32-40
CSN6	Santa Cruz	sc47965	34
USP5	Santa Cruz	sc366624	96
USP7	Santa Cruz	sc30164	135
USP32	Santa Cruz	sc374465	130-190
USP47	Santa Cruz	sc100633	157
FBXO2	Santa Cruz	sc393873	42
FBXO29	Santa Cruz	sc514385	60-70
Ure-b1	Santa Cruz	sc49768	400
Six4	Santa Cruz	sc55766	80
Smad4	Santa Cruz	sc7966	60
Nek9	Santa Cruz	sc50765	120
NRK1	Santa Cruz	sc398852	25
HSP70	Enzo	ADI-SPA-810	70
Hsc70	Enzo	ADI-SPA-815	71
ROMK	Novus	NBP1-82874	45
CHIP (Stub1)	Novus	NBP2-47510	35
AQP4	Alamone	AQP-004	30
Actin	Sigma-Aldrich	A2228	42
AQP2 9398	N/A	Moeller HB, Aroankins TS, Slengerik-Hansen J, Pisitkun T, Fenton RA: Phosphorylation and ubiquitylation are opposing processes that regulate endocytosis of the water channel aquaporin-2. <i>J Cell Sci</i> 127: 3174-3183, 2014	25 and 35-45
pS256-AQP2	N/A	Hoffert JD, Fenton RA, Moeller HB, Simons B, Tchapyjnikov D, McDill BW, Yu MJ, Pisitkun T, Chen F, Knepper MA: Vasopressin-stimulated increase in phosphorylation at Ser269 potentiates plasma membrane retention of aquaporin-2. <i>J Biol Chem</i> 283: 24617-24627, 2008	25 and 35-45
NKCC2	N/A	Ecelbarger CA, Terris J, Hoyer JR, Nielsen S, Wade JB, Knepper MA. Localization and regulation of the rat renal Na(+)-K(+)-2Cl ⁻ cotransporter, BSC-1. <i>Am J Physiol</i> 271: F619-F628, 1996	140
pNKCC2	N/A	Dimke H, et al. Acute growth hormone administration induces antidiuretic and antinatriuretic effects and increases phosphorylation of NKCC2. <i>Am J Physiol Renal Physiol</i> 292: F723-F735, 2007	140
NHE3	N/A	Kim GH, Ecelbarger C, Knepper MA, Packer RK. Regulation of thick ascending limb ion transporter abundance in response to altered acid/base intake. <i>J Am Soc Nephrol</i> 10: 935-942, 1999	75
NaKATPase (α1 subunit)	N/A	Kashgarian, M., Biemesderfer, D., Caplan, M., and Forbush, B. 3rd.. Monoclonal antibody to Na,K-ATPase: immunocytochemical localization along nephron segments. <i>Kidney Int</i> 28: 899-913, 1985	90
Alpha-ENaC	N/A	Sorensen MV, et al. Rapid dephosphorylation of the renal sodium chloride cotransporter in response to oral potassium intake in mice. <i>Kidney Int</i> 83: 811-824, 2013	90 and 25 (cleaved)
Gamma-ENaC	N/A	Masilamani S, Kim GH, Mitchell C, Wade JB, Knepper MA. Aldosterone-mediated regulation of ENaC alpha, beta, and gamma subunit proteins in rat kidney. <i>J Clin Invest</i> 104:R19-R23, 1999	85



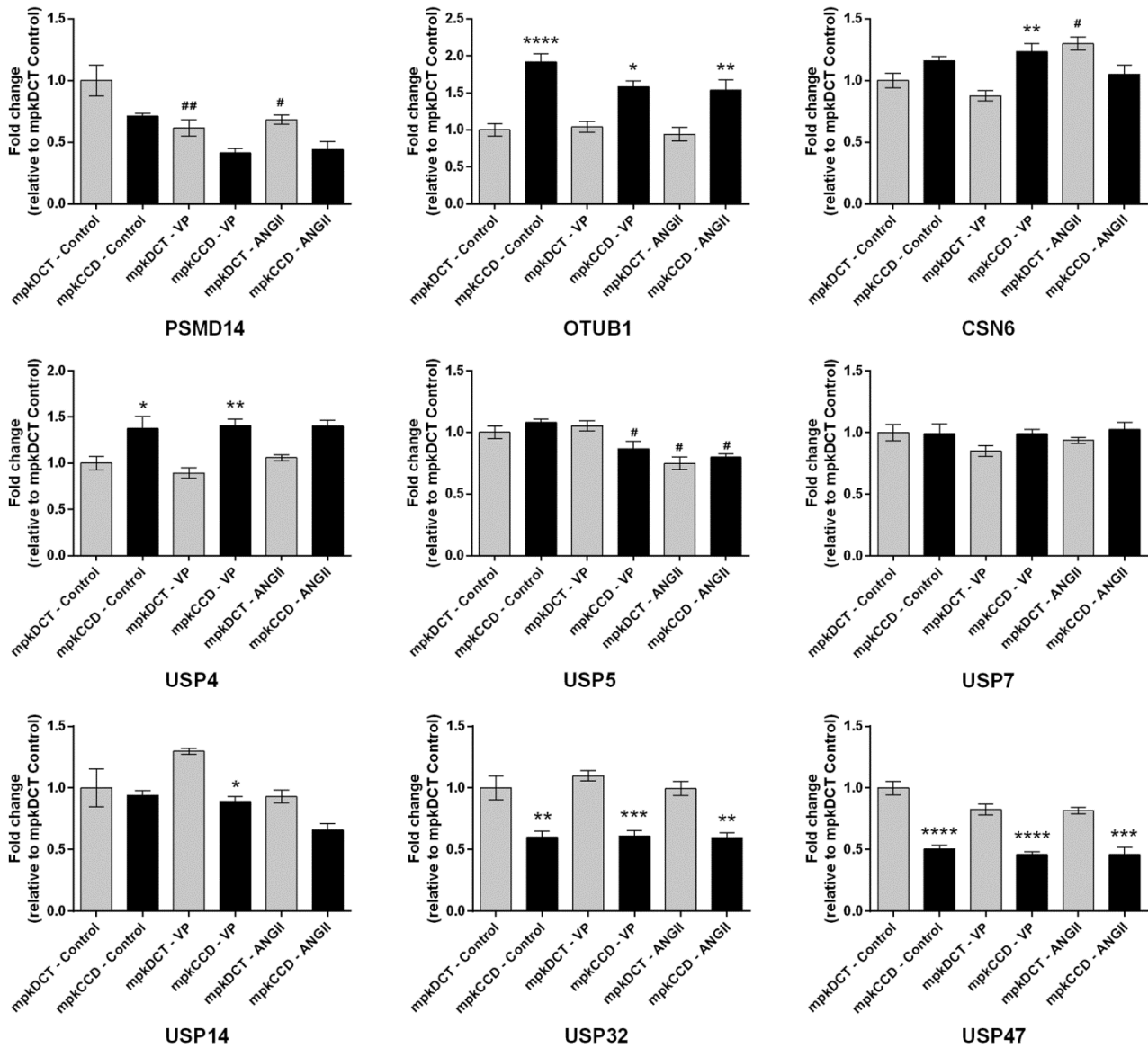
Supplemental Figure 1. Proteomics experimental workflow. mpkDCT cells were cultured in heavy SILAC medium (Lys+6, Arg+10) while mpkCCD cells in light SILAC medium (Lys+0, Arg+0). Four passages of labelled cells were used to generate four biological replicates for statistical analysis. In addition to control conditions, cells were also stimulated for 4 days with the vasopressin type II receptor agonist 1-desamino-8-D-arginine vasopressin (dDAVP, 1nM, only to basolateral (baso) side) or angiotensin-2 (ANGII, 1nM, to both apical and basolateral sides). Cells were harvested, equally pooled and subjected to offline high-pH fractionation based two dimensional LC-MS/MS analysis (Q-Exactive).



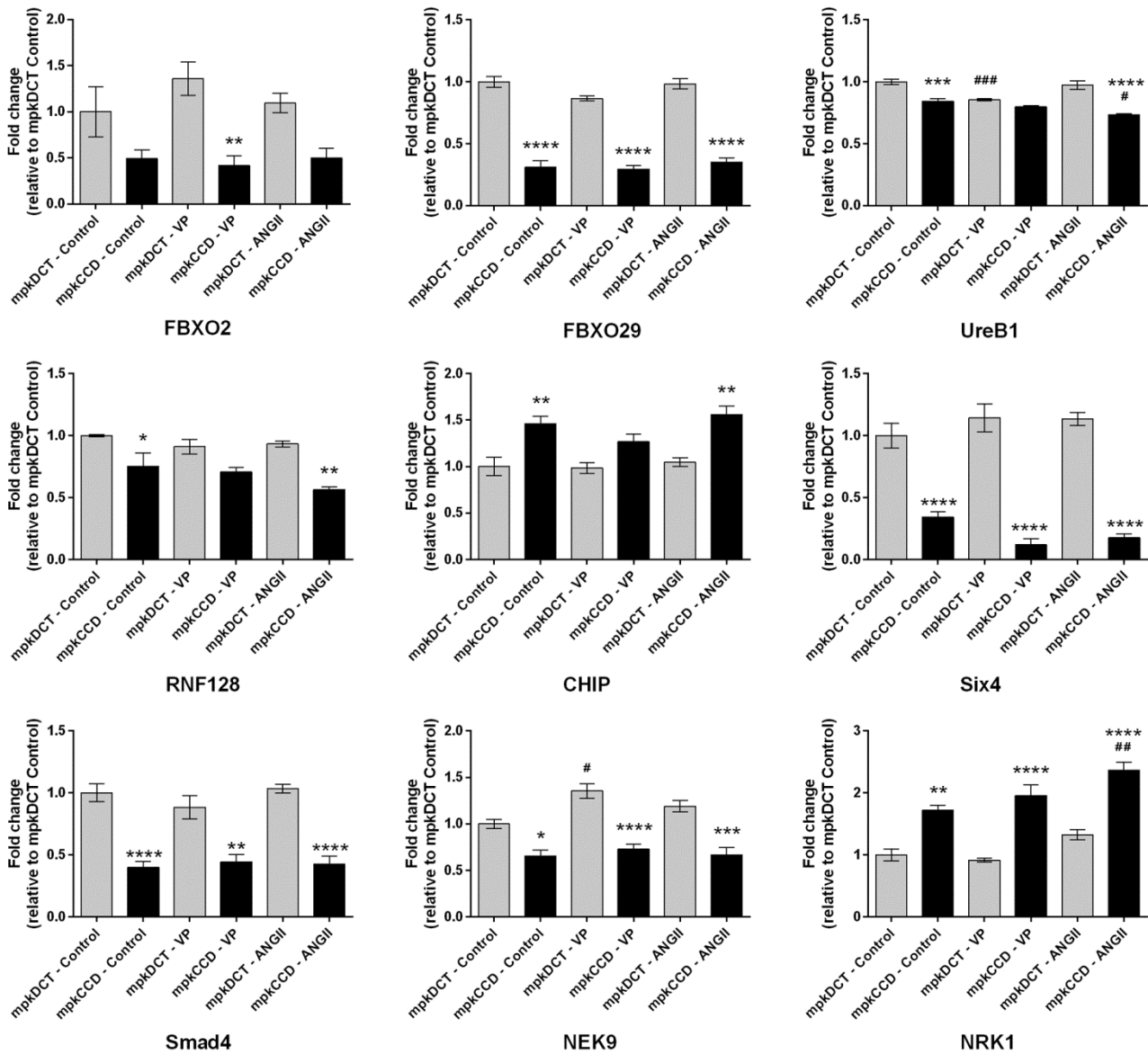
Supplemental Figure 2. Loading controls for immunoblotting of mpkDCT and mpkCCD cells. Equal protein equivalents of samples isolated from the different cell types and different treatments were used for subsequent immunoblotting as demonstrated by Coomassie gel (A) or immunoblot of actin (B).



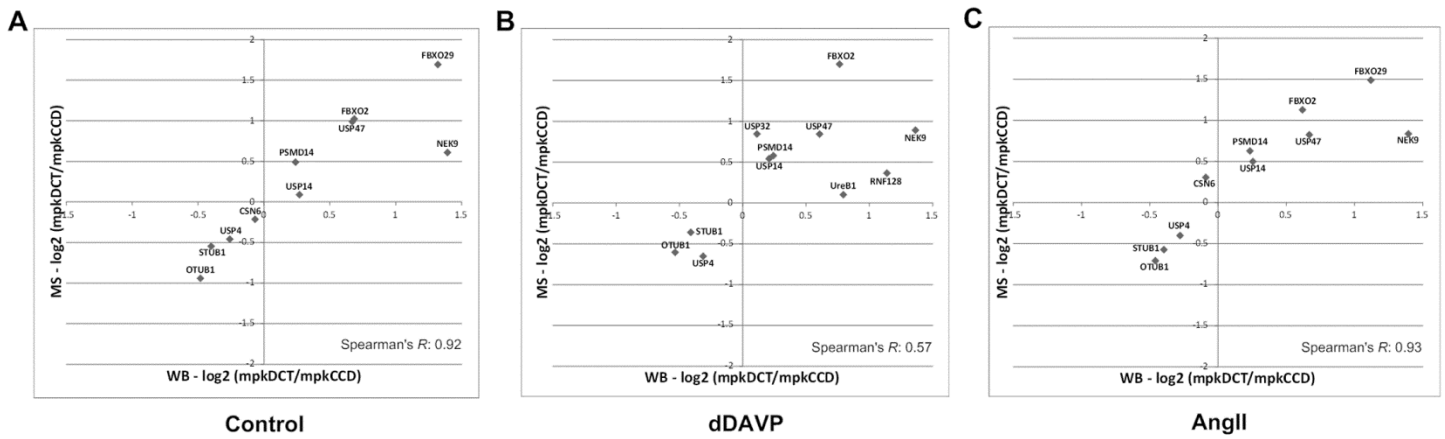
Supplemental Figure 3. Immunoblotting for a variety of the regulatory proteins identified in mpkDCT or mpkCCD cells. Specificity of the commercial antibodies was based on that they either gave a single unique band on an immunoblot corresponding to the target proteins predicted molecular weight, or the most prominent band on the immunoblot was at the target proteins predicted molecular weight (with no other bands of similar size).



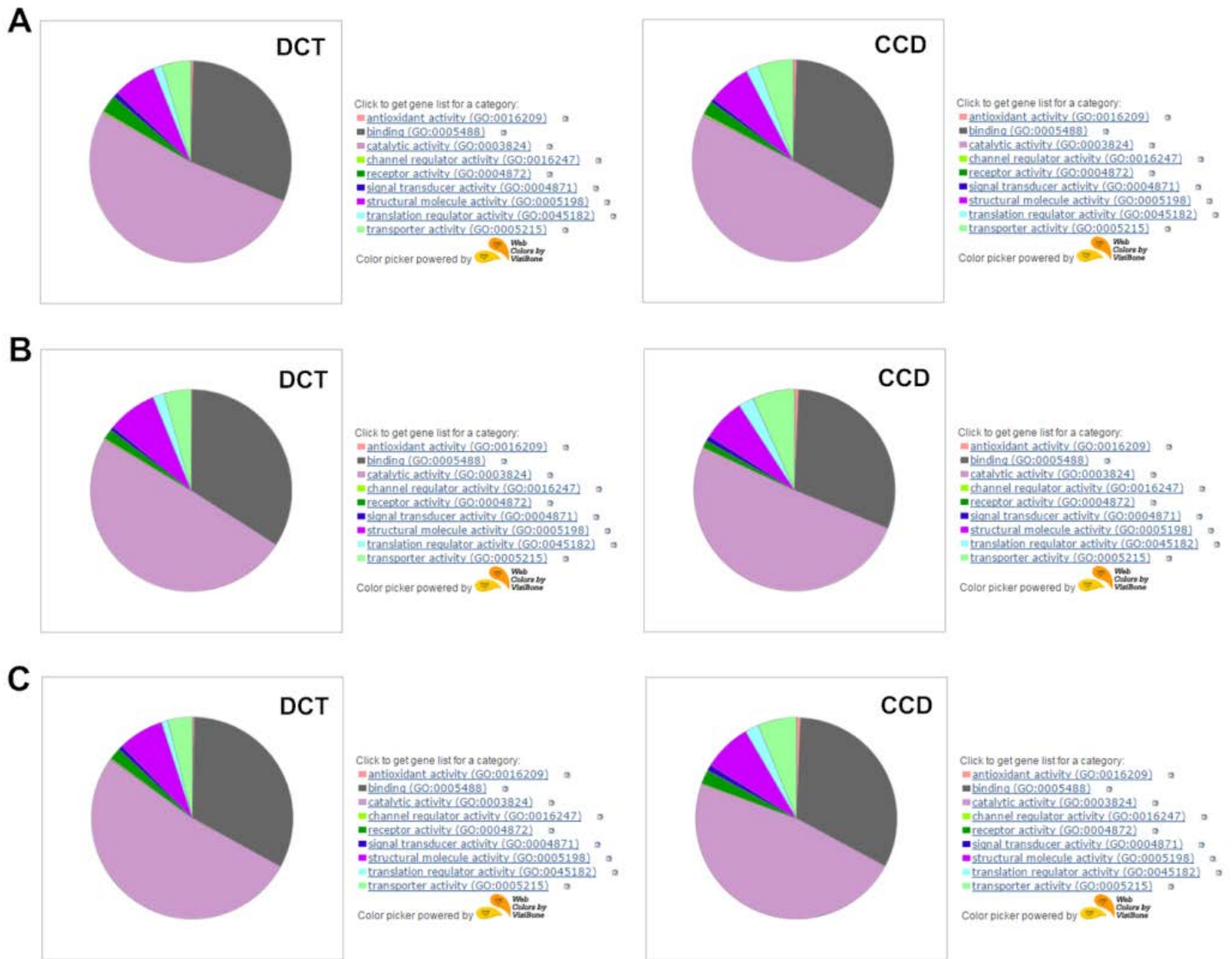
Supplemental Figure 4. Immunoblot quantification of selected DUB genes in mpkDCT and mpkCCD cells grown under three conditions. The mpkDCT control condition was set as baseline, and all other quantifications were relative to mpkDCT control condition. * denotes significance between DCT and CCD under the same condition (DCT used as reference) while # denotes significance within one cell type under different conditions (control condition used as reference). * or #: 0.01<p<0.05; ** or ##: 0.001<p<0.01; *** or ###: 0.0001<p<0.001; **** or ####: p<0.0001.



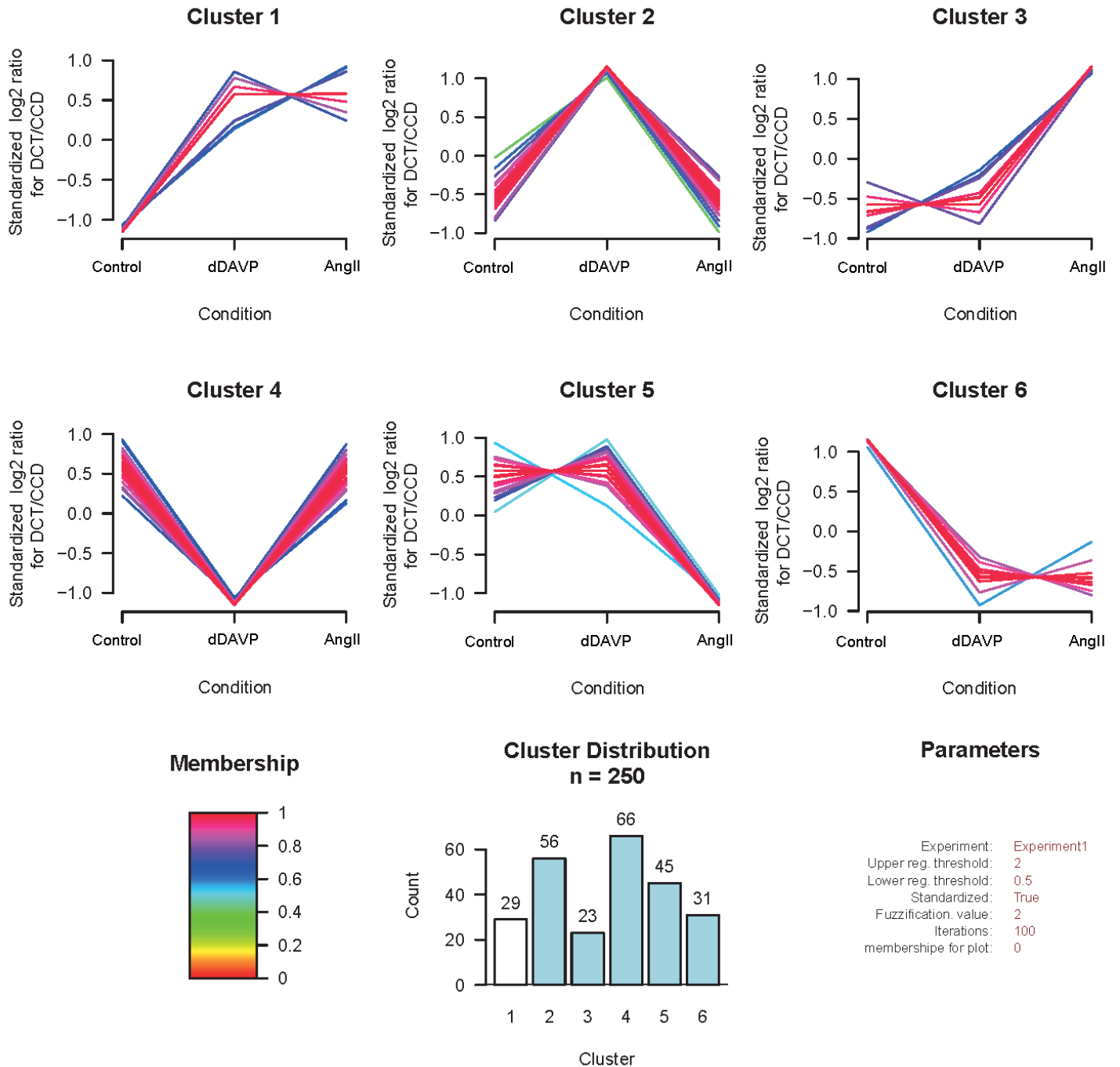
Supplemental Figure 5. Immunoblot quantification of selected kinase, E3 ligase and TF genes in mpkDCT and mpkCCD cells grown under three conditions. The mpkDCT control condition was set as baseline, and all other quantifications were relative to mpkDCT control condition. * denotes significance between DCT and CCD under the same condition (DCT used as reference) while # denotes significance within one cell type under different conditions (control condition used as reference). * or #: 0.01<p<0.05; ** or ##: 0.001<p<0.01; *** or ###: 0.0001<p<0.001; **** or ####: p<0.0001.



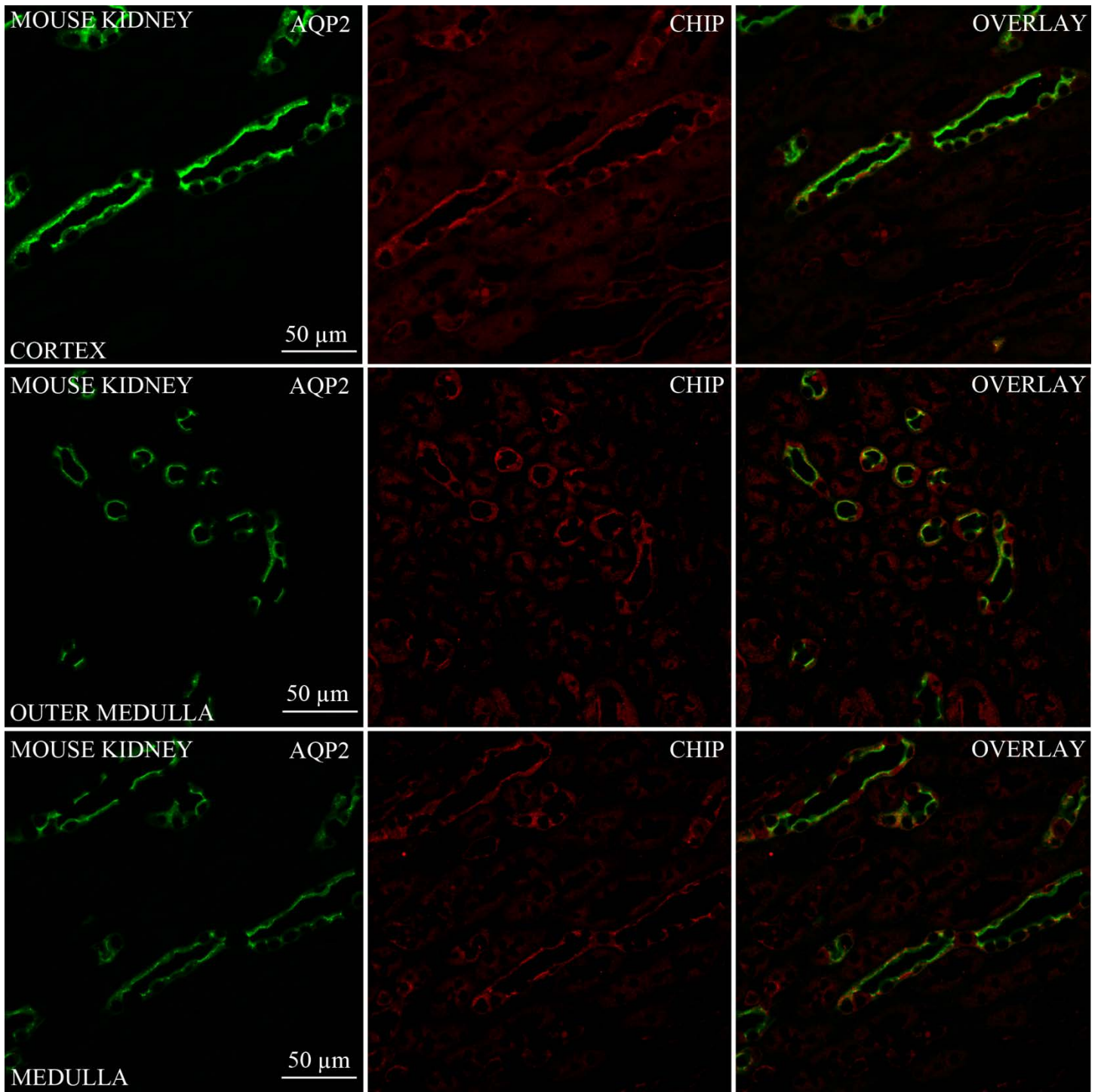
Supplemental Figure 6. The correlation between immunoblot based quantification and mass spectrometry based quantification for selected genes in mpkDCT and mpkCCD cells grown under three conditions. (A) Control condition; (B) dDAVP treatment; (C) AngII treatment. The spearman's correlation coefficient was calculated for each condition.



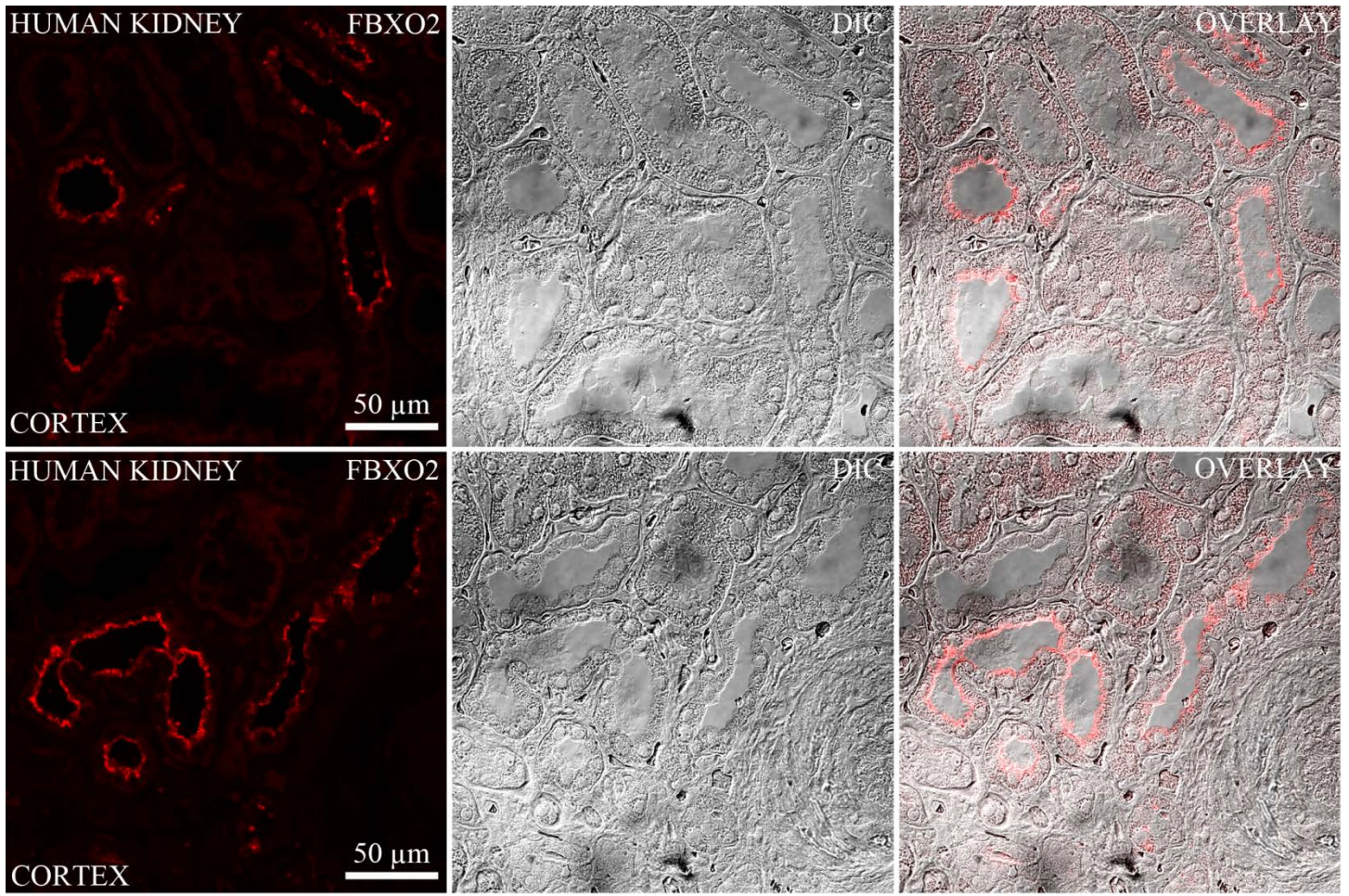
Supplemental Figure 7. GO-term molecular function analysis by Panther. (A) Control condition; (B) dDAVP treatment; (C) AngII treatment. Cell specific genes under each condition were used as Panther inputs.



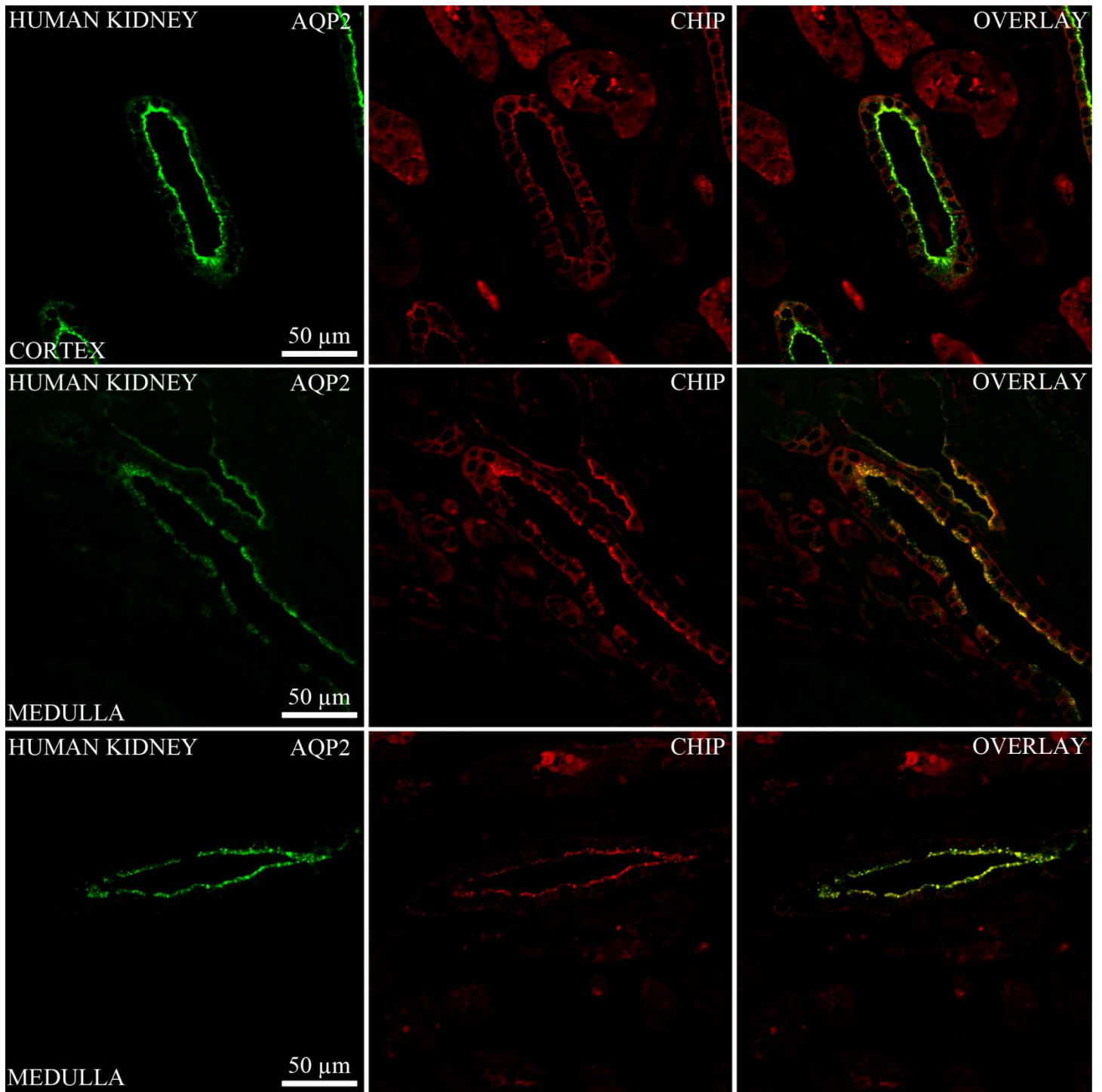
Supplemental Figure 8. Cluster analysis of 250 proteins with the largest standard deviations under three conditions showed 6 distinctive clusters. The data indicates that dDAVP and AngII can have similar – or independent – effects on a subset of proteins in mpkDCT or mpkCCD cells. For example, the abundance of proteins in Clusters 2 and 4 are specifically regulated by dDAVP (but not by AngII), the abundance of proteins in Clusters 3 and 5 are specifically regulated by AngII (but not by dDAVP), whereas the abundance of proteins in Clusters 1 and 6 can be regulated by both dDAVP or AngII.



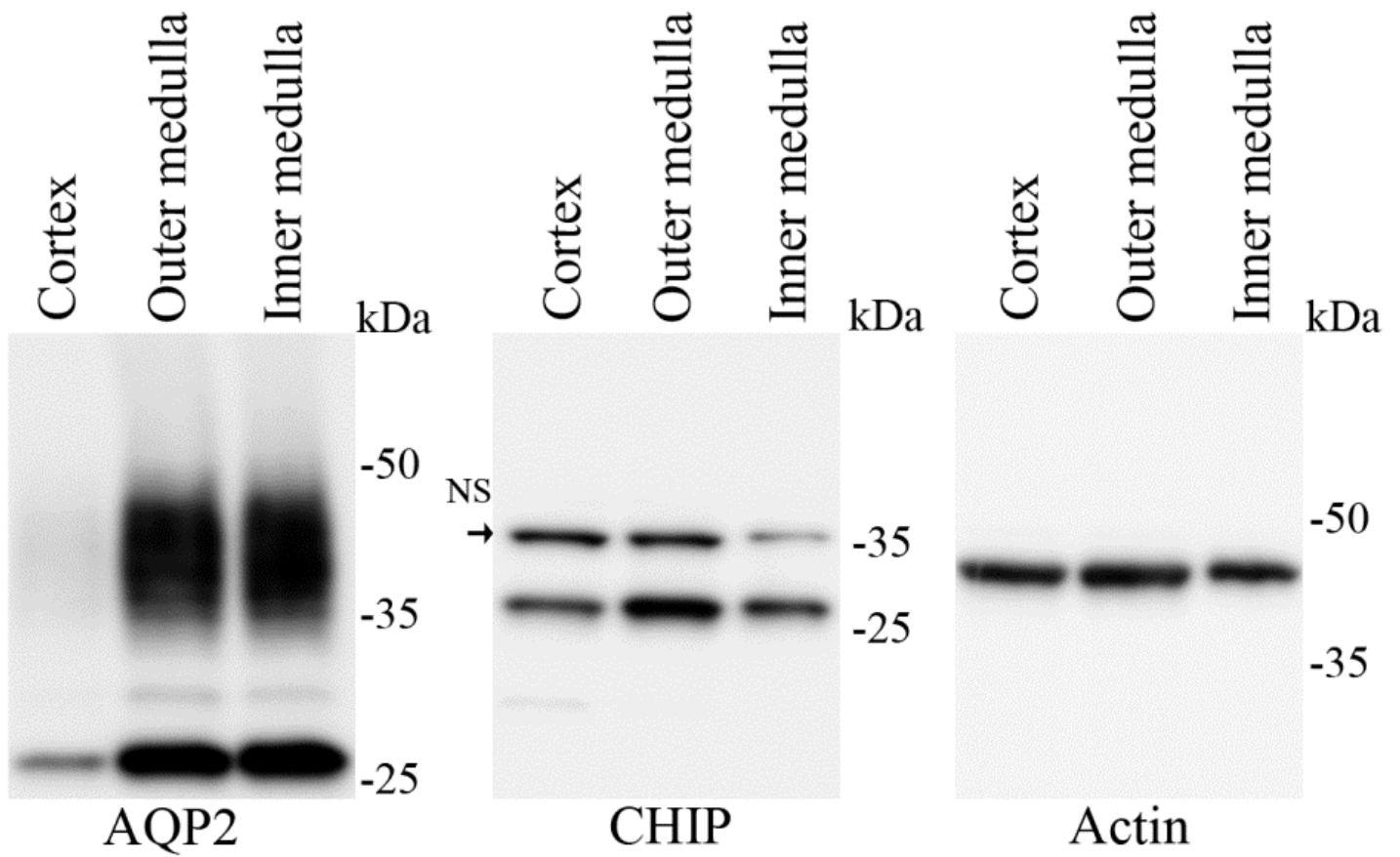
Supplemental Figure 9. Immunohistochemical localization of CHIP in mouse kidney. Confocal images of CHIP and AQP2 distribution in mouse kidney cortex, outer medulla and medulla. CHIP is expressed in principal cells throughout the collecting duct system where it partially colocalizes with AQP2.



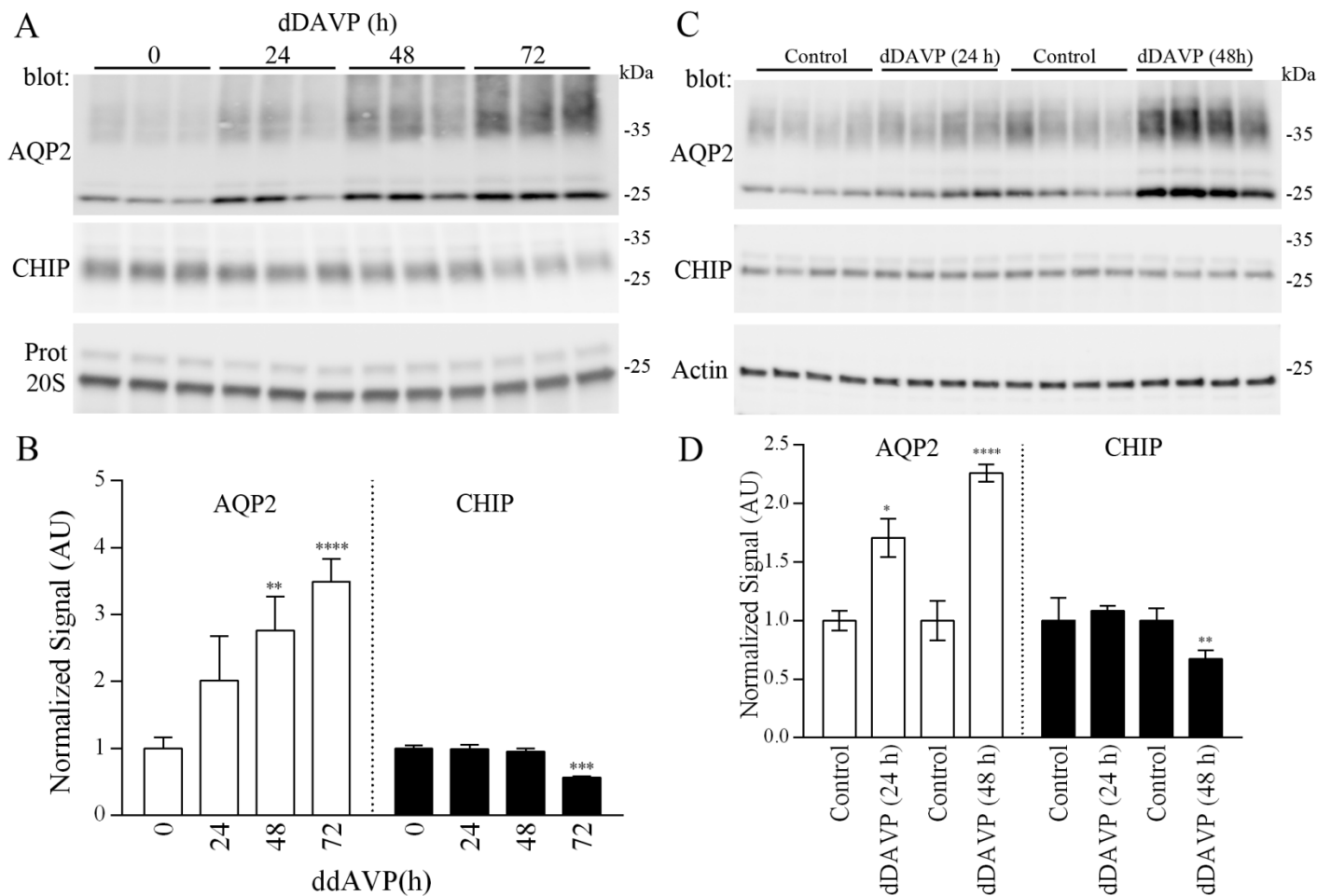
Supplemental Figure 10. Immunohistochemical localization of FBXO2 in human kidney. Confocal images of FBXO2 distribution in human kidney cortex. Differential interference contrast (DIC) images are provided to demonstrate the structure of the imaged section. FBXO2 is localized to tubules morphologically resembling the DCT.



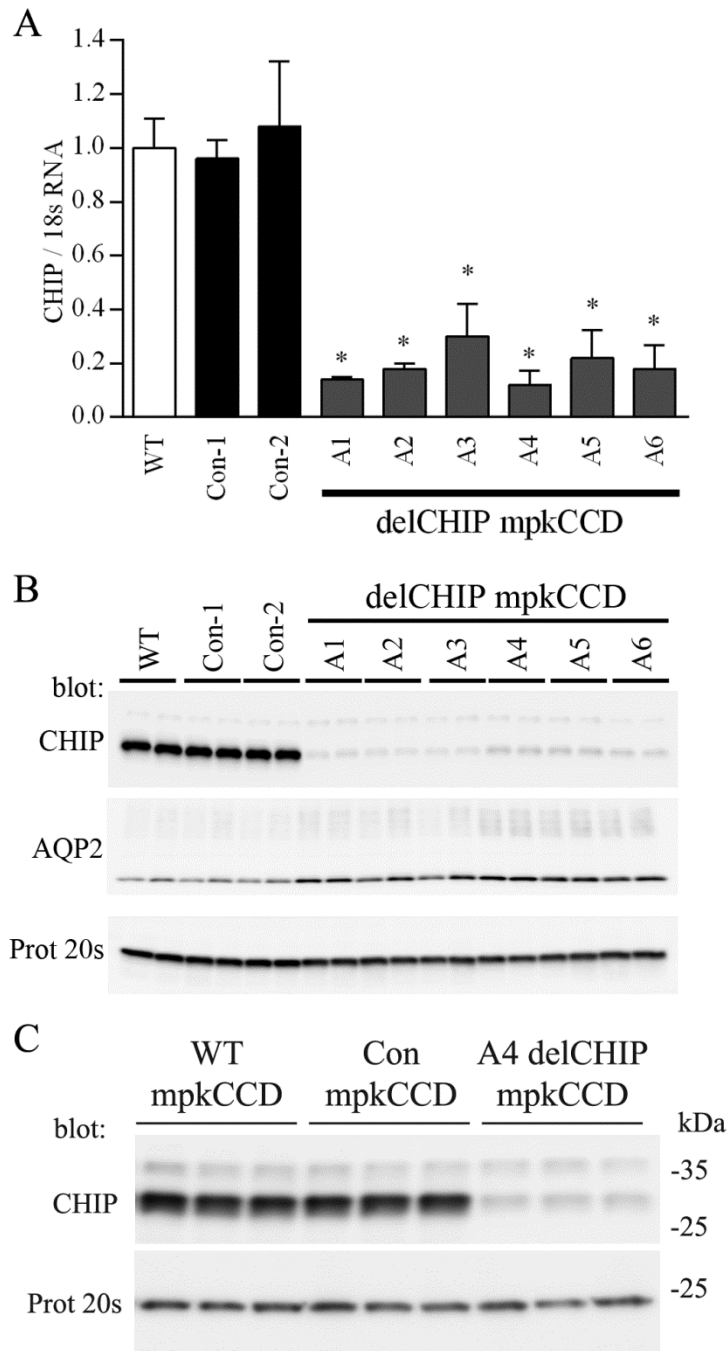
Supplemental Figure 11. Immunohistochemical localization of CHIP in human kidney. Confocal images of CHIP and AQP2 distribution in human kidney cortex and medulla. CHIP is expressed in collecting duct principal cells where it partially colocalizes with AQP2.



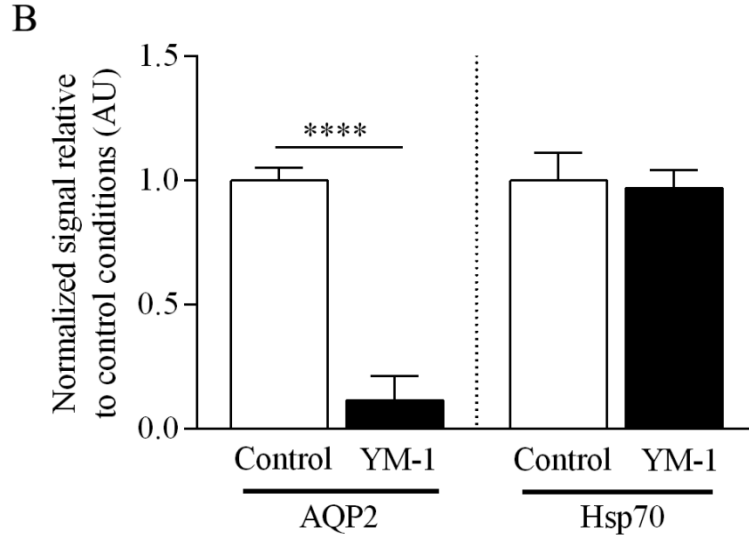
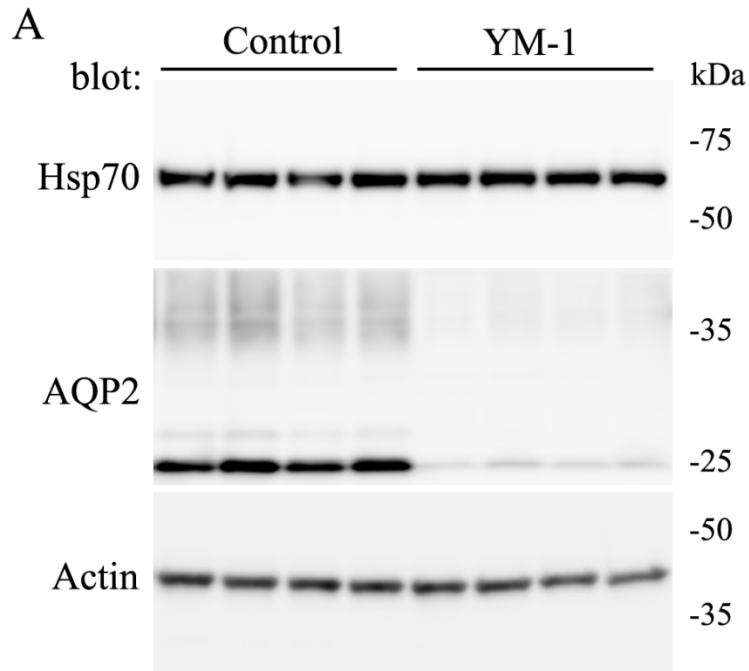
Supplemental Figure 12. CHIP distribution in different mouse kidney zones. Immunoblotting of total protein homogenates isolated from mouse kidney cortex, outer medulla and inner medulla demonstrate that CHIP is abundantly expressed in all regions examined. AQP2 is more abundant in the outer medulla and inner medulla. Immunoblotting for actin serves as a loading control.



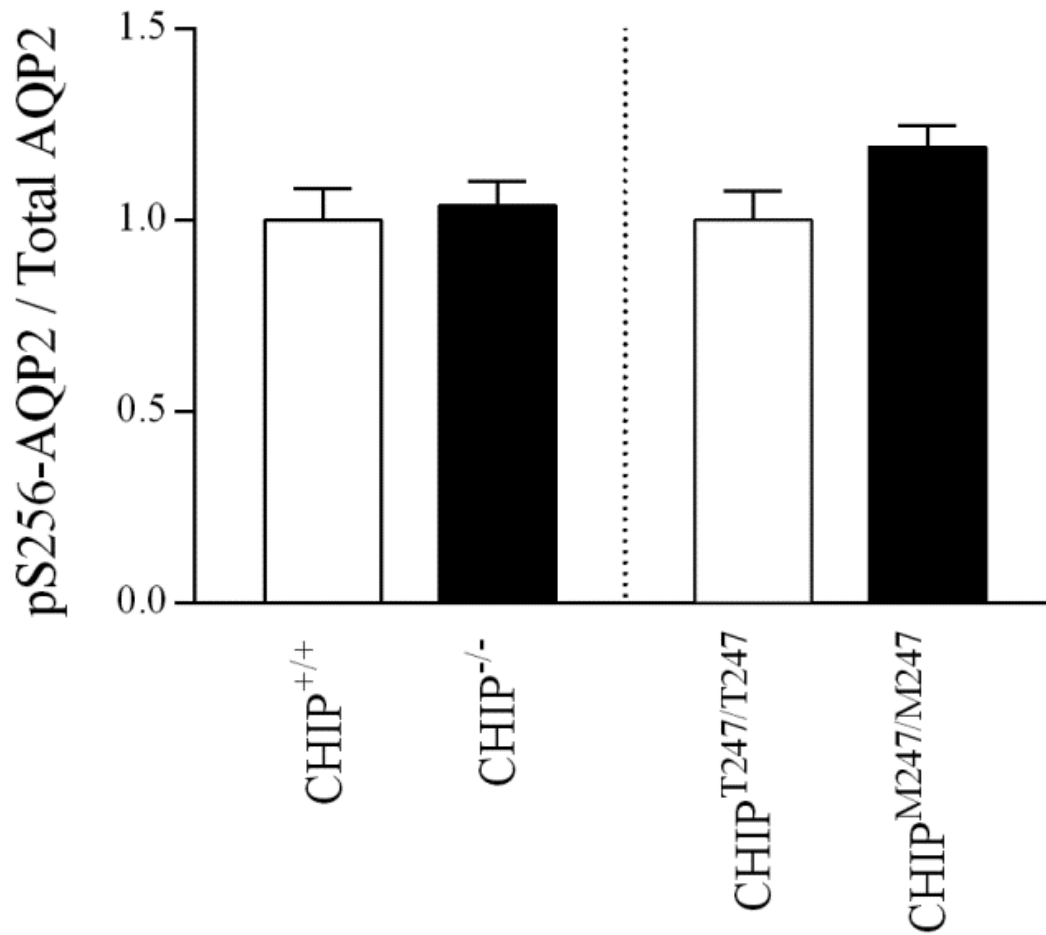
Supplemental Figure 13. *In vitro* and *in vivo* effects of dDAVP on CHIP and AQP2 abundance. A) Representative immunoblots of AQP2 and CHIP following dDAVP treatment of mpkCCD cells. B) Semi-quantitative summary of data. * indicates significance relative to 0 h time point. C) Representative immunoblots of AQP2 and CHIP in mice kidneys following dDAVP treatment of mice. Each lane represents an individual mouse sample. D) Semi-quantitative summary of data. * indicates significance relative to time-matched control group. *: $0.01 < p < 0.05$; **: $0.001 < p < 0.01$; ***: $0.0001 < p < 0.001$; ****: $p < 0.0001$.



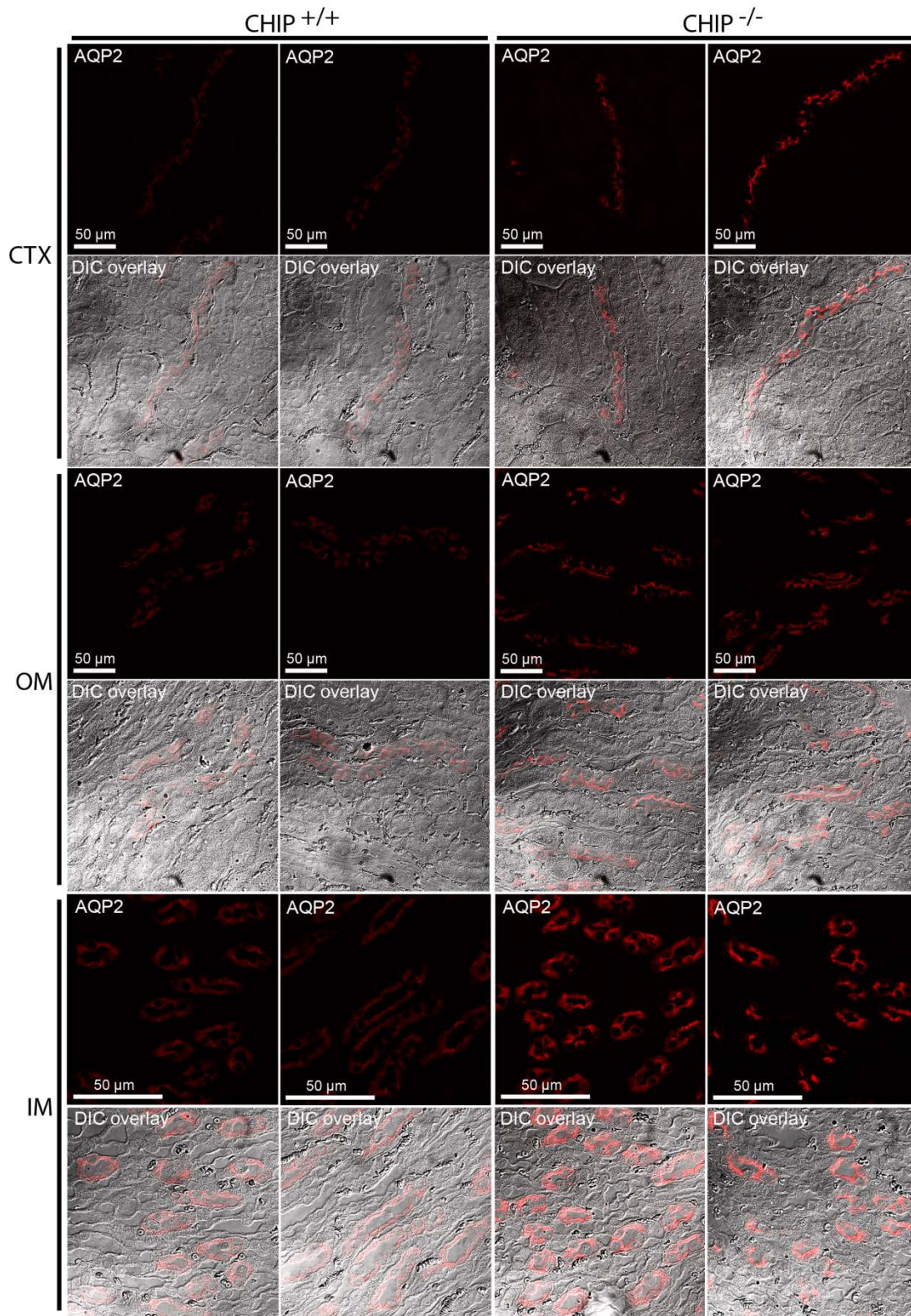
Supplemental Figure 14. Initial characterization of CHIP knockdown mpkCCD cells. A) RT-qPCR detection of CHIP mRNA levels in various lentivirus transduced CHIP shRNA expressing mpkCCD cells (A1-A6 delCHIP). Significant reductions in CHIP mRNA levels are observed in all the individual delCHIP lines relative to wildtype (WT) mpkCCD cells or scrambled shRNA control cells. B) Immunoblotting of CHIP demonstrates a clear reduction of CHIP protein in the A1-A6 delCHIP lines relative to wildtype (WT) mpkCCD cells or scrambled shRNA control cells. In each line the decrease in CHIP correlates with increased levels of AQP2. C) The A4delCHIP cells were used for the remainder of studies and showed a consistent reduction in CHIP protein levels relative to WT or scrambled shRNA expressing Con mpkCCD cells.



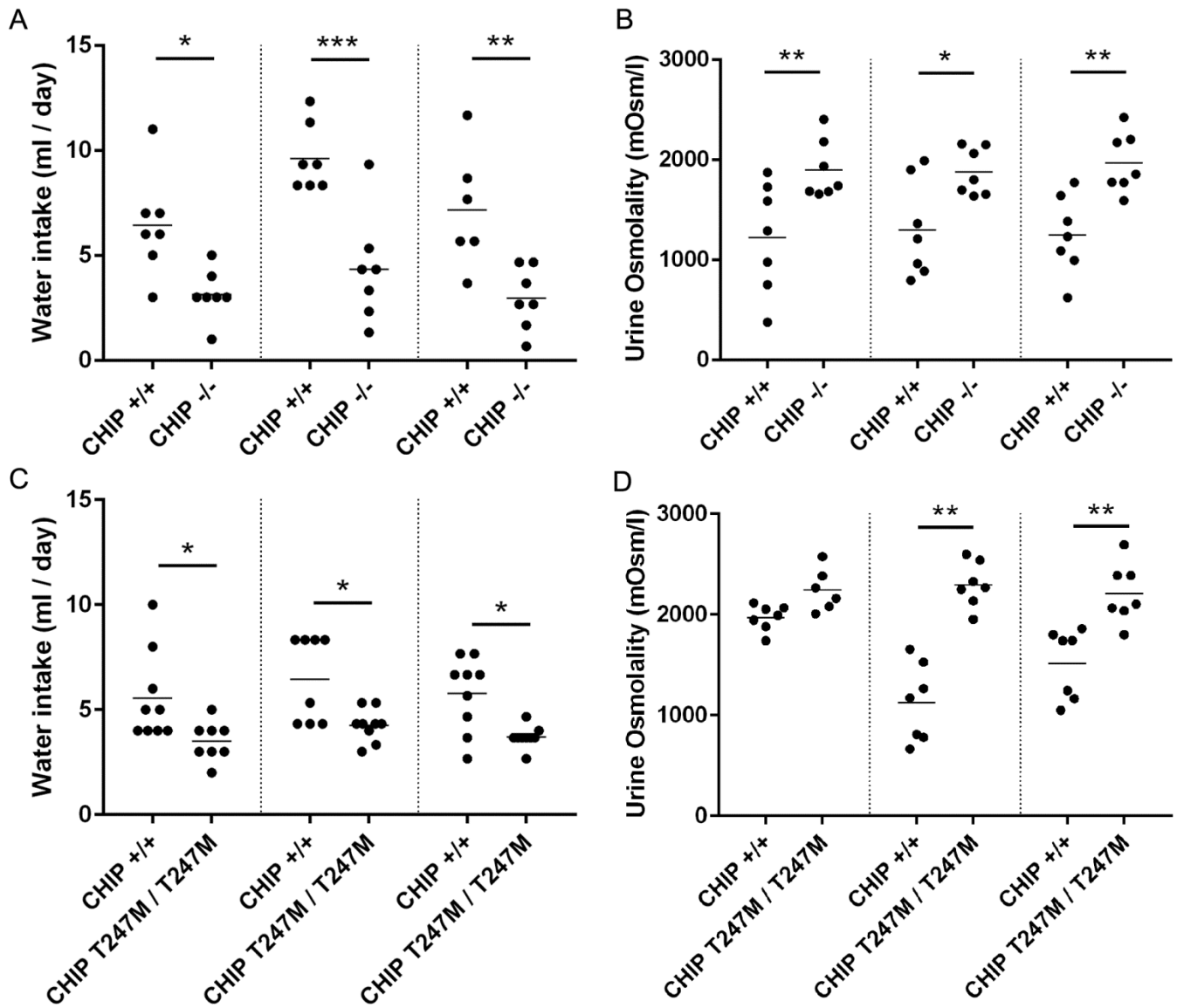
Supplemental Figure 15. Treatment of control mpkCCD cells with the Hsp70 activator YM-1 significantly reduces AQP2 levels. A) Immunoblotting of AQP2, Hsp70 and actin in samples isolated from cells treated with YM-1, which activates Hsp70 in a similar manner to Hip and stabilizes Hsp70 in its ADP-bound conformation favoring degradation of misfolded substrates. AQP2 levels are substantially reduced, strengthening the role of an Hsp70/CHIP dependent AQP2 degradation mechanism. Hsp70 levels are not affected by YM-1 treatment. Actin serves as a loading control. B) Quantification of AQP2 and Hsp70 in control and YM-1 treated mpkCCD cells. Values are obtained from 3 independent experiments with $n = 3-4$ for each individual treatment. * denotes significance between control and YM-1 treated cells. ****: $p < 0.0001$.



Supplemental Figure 16. pS256-AQP2 levels are not significantly greater in CHIP^{-/-} and CHIP^{M247/M247} mice when total AQP2 levels are considered. Summary of data from CHIP^{+/+} mice and CHIP^{-/-} mice (n=10/genotype) demonstrating that when normalized to total AQP2 the levels of pS256-AQP2 are not different between the genotypes. Similar results are observed for the CHIP^{M247/M247} and CHIP^{T247/T247} mice (n=6/genotype).



Supplemental Figure 17. Immunolabelling of AQP2 in kidneys from CHIP^{+/+} and CHIP^{-/-} mice. Images are representative confocal images of AQP2 expression in kidney sections from the kidney cortex, outer medulla and inner medulla of CHIP^{+/+} and CHIP^{-/-} mice. AQP2 levels were increased throughout the collecting duct in CHIP^{-/-} mice, with apical labeling being more apparent. Differential interference contrast (DIC) images are provided to demonstrate the structure of the imaged section. A Leica TCS SL confocal microscope with an HCX PL APO 63x oil objective lens (numerical aperture: 1.40) was used with identical microscope settings (PMT offset and gain, sampling period, and averaging) for obtaining images. The dynamic range of the image acquisition was set so that the sections with the most intense fluorescence signal only had a few saturated pixels.



Supplemental Figure 18. Baseline renal water handling of CHIP^{-/-} and CHIP^{M247/M247} mice. A) CHIP^{-/-} mice had decreased fluid intake on three successive days. B) The osmolality of spontaneously voided urine from CHIP^{-/-} mice was significantly higher on each recorded day. C) CHIP^{M247/M247} mice had decreased fluid intake on three successive days. D) The osmolality of spontaneously voided urine from CHIP^{M247/M247} mice was significantly higher on the last two recorded days. * denotes significance between CHIP^{+/+} and CHIP^{-/-} or CHIP^{T247M/T247M} mice. *: 0.01 < p < 0.05; **: 0.001 < p < 0.01; ***: 0.0001 < p < 0.001.

Supplemental Detailed Methods

Cell culture and SILAC labeling. mpkDCT and mpkCCD cells were grown at 37°C/5%CO₂ in SILAC advanced DMEM/F12-Flex media (Invitrogen) containing 60 nM sodium selenite, 5 µg/ml transferrin, 2 mM glutamine, 50 nM dexamethasone, 1 nM triiodothyronine, 10 ng/ml epidermal growth factor, 5 µg/ml insulin, 20 mM D-glucose and 20 mM HEPES (pH 7.4) in light (mpkCCD; contains ¹²C6 lysine, ¹²C6 ¹⁴N4 arginine, for mpkCCD) or heavy (mpkDCT; contains ¹³C6 lysine, ¹³C6 ¹⁵N4 arginine, for mpkDCT) conditions for at least 5 passages to allow >97% labeling efficiency as confirmed by MS analysis. For experiments, cells were grown on semi-permeable supports (Transwell, Corning) until polarized monolayers were formed (transepithelial resistance (TER) >5 kΩ.cm²). Cells were subsequently cultured in serum-free media (media changed every 12 h) in the following groups; 1) Control, 2) 1 nM [deamino-Cys1,D-Arg8]vasopressin (dDAVP) (10⁻⁹ M, Sigma) to only the basolateral side; 3) 1nM AngII (Sigma). After 4 days, cells were washed twice in ice-cold PBS and scraped in cell lysis buffer (8 M urea, 2 M thiourea, 50 mM Tris, pH 7.5) containing protease and phosphatase inhibitors (Halt protease and phosphatase inhibitors, Pierce). After 20 min incubation, lysates were sonicated on ice and centrifuged at 16,000g for 10 min at 4°C. Supernatant protein concentration was measured by Bradford assay (Biorad), and equal protein amounts from mpkDCT and mpkCCD samples within each treatment group were pooled together. Per condition, four independent passages of cells were compared. Pooled samples were reduced, alkylated, and digested with trypsin and subjected to further high-pH reversed phase fractionation ¹.

High-pH reversed phase fractionation. Peptides were loaded onto a ZORBAX Extend-C18 reversed phase column (Agilent, 3.5µm particle size, 4.6 x 150mm) and fractionated using Ultimate 3000 Liquid Chromatography (LC) (Dionex). Buffer A was 25mM NH₄FA in 100% H₂O

(pH adjusted to 9.5 with $\text{NH}_3\cdot\text{H}_2\text{O}$) and buffer B was 25mM NH_4FA in 10% $\text{H}_2\text{O}/90\%\text{ACN}$ (equal volume of $\text{NH}_3\cdot\text{H}_2\text{O}$ added as in buffer A). The fractionation was done by a linear gradient of 2-35% buffer B for 56 min plus a linear gradient of 35-80% buffer B for 8 min. One fraction was collected every 2 minutes, so there were 32 fractions in total. These 32 initial fractions were then combined into 8 final fractions through combining 4 fractions with the same time interval into one e.g. fractions 1, 9, 17 and 25 were pooled into final fraction 1. The final fractions were vacuum-dried and stored in -20°C until MS analysis.

Nano-liquid chromatography and mass spectrometry (nLC-MS) analysis. Fractionated peptides were analyzed by nano Liquid-Chromatography (nLC) (Easy LC 1000, Thermo Scientific) coupled to a Q-Exactive mass spectrometer (Thermo Scientific) through an EASY-Spray nano-electrospray ion source (Thermo Scientific). A pre-column (Acclaim®PepMap 100, $75\ \mu\text{m} \times 2\ \text{cm}$, C18, $3\ \mu\text{m}$, $100\ \text{Å}$, Thermo Scientific) was used to trap peptides and an analytical column (EASY-Spray Column, PepMap, $75\ \mu\text{m} \times 15\ \text{cm}$, C18, $3\ \mu\text{m}$, $100\ \text{Å}$, Thermo Scientific) was used to separate peptides. Buffer A was $100\%\text{H}_2\text{O}/0.1\%\ \text{FA}$ and buffer B was $100\%\ \text{ACN}/0.1\%\ \text{FA}$. A 36-minutes linear gradient from 5% to 35% buffer B was used to separate peptides. MS settings were as follows: full scans (m/z 300-1800) were performed at a resolution of 70,000 with an automatic gain control (AGC) threshold of $3\text{e}6$, a maximum injection time (IT) of 100ms, and 12 data dependent MS/MS scans at a resolution of 17,500 with AGC of $1\text{e}5$ and IT of 50ms. HCD collision energy was 28%. Dynamic exclusion was set at 30 s, and precursor ions with charge state unknown, +1 and above +8 were excluded for fragmentation.

MS data analysis. Identification and quantification were done by MaxQuant (version 1.5.2.8). Raw files from each biological replicate under each treatment condition were searched together

to generate a combined result. Data were searched against RefSeq mouse database (58513 sequences, downloaded Oct. 2014) plus normal contaminants. Multiplicity was set to 2, with Arg10 and Lys6 as heavy labels. Acetylation of Protein N-term, oxidation of methionine, and phosphorylation of serine, threonine and tyrosine were set as variable modifications, and they were also included in protein quantification. iBAQ calculation was turned on. All other parameters, including precursor and fragment mass tolerances, were set as default values of MaxQuant. Proteins that were identified and quantified in at least three biological replicates were regarded as quantifiable proteins and subjected to Benjamini-Hochberg (BH) FDR estimations, and up-regulated proteins in one cell type (mpkDCT or mpkCCD) that passed 1% BH-FDR threshold were regarded as enriched proteins in that cell type. Proteins that had valid iBAQ values in one labeling channel (heavy or light) in at least three biological replicates and “zero” iBAQ values in the other channel in all replicates were regarded as unique proteins in either mpkDCT (heavy channel) or mpkCCD (light channel). The enriched plus unique proteins for each cell type (mpkDCT or mpkCCD) were defined as “specific” proteins for that cell type and retained for further analysis.

The Database for Annotation, Visualization and Integrated Discovery (DAVID) analysis.

mpkDCT and mpkCCD specific proteins were subjected to DAVID (v6.7) functional annotation analysis. mpkDCT and mpkCCD specific protein accessions were transformed to gene symbols using Automated Bioinformatics Extractor (ABE) ² and used as separate inputs. A customized background, containing all the protein accessions identified in this study, was used instead of the default *Mus musculus* background. In order for the DAVID to recognize as many background accessions as possible, the original RefSeq protein accessions were transformed to UniProt accessions using the ID Mapping tool from UniProt (<http://www.uniprot.org/uploadlists/>). Functional annotation clustering with default settings was performed separately on mpkDCT and

mpkCCD specific proteins against the customized background. Annotation clusters between mpkDCT and mpkCCD that share 50% or above individual annotations were mapped together and deemed identical, and a cluster name was given for each mapped cluster. Mapped clusters that had enrichment *p*-values no greater than 0.1 (corresponding to enrichment score no smaller than 1) in either mpkDCT or mpkCCD were retained to generate a heatmap, to illustrate which functions are more enriched in one cell type compared to the other.

Isolation of Enhanced Green Fluorescent Protein (EGFP) expressing mouse DCT cells. All animal protocols were performed in accordance to licenses for the use of experimental animals issued by the Danish Ministry of Justice. Mice had free access to standard rodent chow and water. Transgenic mice expressing EGFP driven by the parvalbumin promoter ³ were euthanized by cervical dislocation and kidneys quickly removed. The kidneys were sliced into approximately 1 mm pieces and incubated for 40 min in buffer B (125 mM NaCl, 0.4 mM KH₂PO₄, 1.6 mM K₂HPO₄, 1 mM MgSO₄, 10 mM Na-acetate, 1 mM α -ketogluterate, 1.3 mM Ca-gluconate, 5 mM glycine, 30 mM glucose and 5 μ g/mL DNase I (Sigma), pH 7.4) containing 2 mg/ml collagenase B (Roche). Samples were mixed continuously at 850 rpm at 37°C. After 10 min, half of the enzyme solution was removed and replaced with buffer B without collagenase, and samples were incubated for a further 10 min. This procedure was repeated for another 10 min. After a total incubation of 40 min, the tubular suspensions were passed through a 100 μ M cell strainer (BD Falcon), and centrifuged for 3 min at 200 g. Cells were washed with a trypsin/EDTA solution (Lonza) containing 10 mM HEPES, 30 mM glucose and 50 μ g/ml DNase I. Cells were again resuspended in trypsin/EDTA solution and incubated for 15 min at 37°C. Cells were washed in DMEM/HamF12 cell culture medium (Gibco) containing 5% FBS, 30 mM glucose, 10 mM HEPES and 50 μ g/ml DNase I and subsequently resuspended in 1.5 ml medium. Cells were passed through a 40 μ M cell strainer and kept at 4°C. EGFP-positive and

negative cells were isolated on a FACSAria III (BD Biosciences) machine at the FACS Core Facility, Aarhus University, Denmark. Sorted cells were centrifuged for 10 min at 3,000 g at 4°C and the pellet was resuspended in 1x Laemmli sample buffer (62.5 mM Tris, 8.75% Glycerol, 3% SDS, 89.5 μM Bromphenolblue, 15 mg/ml DTT, pH 6.8). Samples were heated for 10 min at 65°C. EGFP purity changed from 4% before sorting to 94% after sorting in the EGFP-positive sample and 0% in the EGFP negative sample.

Antibodies. For western blotting, the antibodies utilized, the supplier and the predicted molecular weight of the target protein are detailed in Supplemental Table 7. Specificity of the commercial antibodies was based on that they either gave a single unique band on an immunoblot corresponding to the target proteins predicted molecular weight, or the most prominent band on the immunoblot was at the target proteins predicted molecular weight (with no other bands of similar size). Other characterized antibodies were AQP2 9398 ⁴ and pS256-AQP2 ⁵.

Fluorescent immunohistochemistry and confocal microscopy analysis. Specimens of human tissue were obtained post-mortem from the pathology archives at Aarhus University Hospital

(<http://www.en.auh.dk/departments/cancer+and+inflammation+centre/department+of+histopathology/research>). Studies on this tissue were performed after approval from the local ethical committee, Aarhus County, Denmark. Archived paraffin-embedded mouse kidney tissue was processed as previously described ⁶. Tissue from the CHIP gene-manipulated mice was immersion fixed in 4% PFA in PBS for 24 h before being processed as previously described ⁶. Sections were immunolabeled for confocal laser scanning microscopy as previously described ⁶

using CSN6 (sc47965), USP32 (sc374465), CHIP (sc133066), FBXO2 (sc393873), AQP2 C17 (sc9882) and NCC (SPC402D, Stressmarq). A Leica TCS SL confocal microscope with an HCX PL APO 63 x oil objective lens (numerical aperture: 1.40) was used for imaging of labelled sections (Leica Microsystems). For qualitative assessment of AQP2 abundance, microscope settings (PMT offset and gain, sampling period, and averaging) were equal for obtaining images. The dynamic range of the image acquisition was set so that the sections with the most intense fluorescence signal only had a few saturated pixels. Brightness was digitally enhanced on presented images.

Generation of mpkCCD cells with stable CHIP knockdown. MISSION lentiviral transduction particles against CHIP (numbers 8527, 8528, 8530, 280520, 280575) and corresponding control particles (SHC002V) were from Sigma. mpkCCD14 cells were cultured as described⁷ in 24-well plates until 95% confluent. Cells were treated with hexadimethrine bromide (8 µg/ml final concentration) for 15 min in pure media, before addition of lentiviral particles (multiplicity of infection = 1.5). Transduction was allowed to proceed for 24 h, after which media was switched to mpkCCD14 media containing 2 µg/ml of puromycin for selection. Multiple clonal cell lines were isolated and individually characterized by examination of cell morphology, high TEER when grown on semi-permeable supports, CHIP expression levels by western blotting and RT-qPCR.

Real time quantitative PCR (RT-qPCR). Total RNA was isolated using the Ambion Ribopure kit (Invitrogen), treated with DNase I (Invitrogen), and reverse transcribed using Superscript II and random primers (Invitrogen); all steps were performed according to the manufacturer's instructions. A control reaction without the reverse transcriptase enzyme was performed to

exclude genomic DNA amplification. Primer pairs utilized spanning an exon-exon junction or an intron were: AQP2 (5'-TGGCTGTCAATGCTCTCCAC and 5'-GGAGCAGCCGGTGAAATAGA); STUB (5'-TCTACCCTCAATTCCGCCTT and 5'-GTGGCAGCGGTCATTGAGAA); 18S RNA (5'-GGATCCATTGGAGGGCAAGT and 5'-ACGAGCTTTTAACTGCAGCAA). Specificity of the amplified products was determined using melting curve-analysis software, gel electrophoresis, and sequencing. Amplification was performed using the cDNA equivalent of 5 ng of RNA, 5 pmol of each primer and either HotStar Taq polymerase (Qiagen) or SYBR Green I Master Taq (Roche Applied Science). Cycling conditions were: 95 °C for 5 min, followed by 40 cycles of 95 °C for 10 s, 60 °C for 20 s, and 72 °C for 30s. RT-qPCR reactions were run on a LightCycler 480 (Roche), with fluorescence measured at the end of each elongation step to calculate Ct values. Relative quantitation of gene expression was determined using the comparative Ct method. Signals for ribosomal 18S RNA amplified in parallel were used to normalize for differences in the amount of starting cDNA.

mpkCCD14 culture and experimental conditions for CHIP analysis. mpkCCD14 cells were cultured on semi-permeable supports (0.4 µM pore size, Corning) until a confluent monolayer formed and TER was above 5 kOhm/cm². 1 nM dDAVP was added in serum-free media to the basolateral compartment for 72 h to induce AQP2 expression. For acute dDAVP stimulation, cells were washed twice in pure media and reincubated in pure media for 3 h before re-stimulated with dDAVP (1 nM) from the basolateral side for 20 min at 37 °C. In dDAVP washout experiments, cells were subsequently washed twice in pure media and reincubated for 30 min at 37 °C before sample preparation. For 17-N-allylamino-17-demethoxygeldanamycin (17-AAG) studies, where indicated cells were incubated with 2µM 17-AAG for 16h before harvest. For Hsp70 activation studies, where indicated cells were incubated with 5 µM 2-[[3-Ethyl-5-(3-methyl-2(3H)-benzothiazolylidene)-4-oxo-2-thiazolidinylidene]methyl]-1-methyl-pyridinium

chloride (YM-1, Sigma) for 16h in the presence of dDAVP before harvest. For proteasomal and lysosomal inhibition experiments, after 72 h of dDAVP treatment, cells were washed twice in pure media and re-incubated in pure media for 8 h in the presence of 10 μ M lactacystin, 150 μ M chloroquine or both, as indicated. For studies examining the long-term effects of ddAVP, cells were incubated with 1 nM dDAVP from the basolateral side for indicate time points. For cycloheximide chase studies, cells were incubated for various time points at 37 °C and 5% CO₂ in 50 μ M cycloheximide. Cells were washed twice in PBS and proteins were extracted in Laemmli sample buffer containing 10 mg/ml of DTT. For calculation of the protein half-life, average band densities for each time point were normalized to control and fitted using nonlinear regression and a one-phase exponential decay equation using GraphPad Prism software. Data were obtained from four independent experiments, with 3–6 observations for each individual time point.

Effects of dDAVP in mice. All animal work has been conducted according to relevant national and international guidelines. Animal housing conditions and experiments were approved by the Danish Ministry of Justice. Care of animals was in accordance with institutional guidelines. Mice were housed individually in metabolic cages and received 1 ng/h dDAVP via osmotic minipump for the indicated timeframes. Control animals received saline vehicle. At the end of the experiment, mice were euthanized by cervical dislocation and the kidneys processed as previously described ⁸.

Surface biotinylation of mpkCCD14 cells. Apical plasma membrane proteins were labeled with EZ-link hydrazide-biotin (Pierce) as previously described ⁹.

Immunoblotting. Standard procedures were utilized for sample preparation and SDS-PAGE. Immunoblots were developed using ECL detection and signal intensity in specific bands were quantified using Image Studio Lite (Qiagen) densitometry analysis.

Immunoprecipitation (IP) using mpkCCD14 cells. IP was performed as previously described⁴.

Mouse models of CHIP dysfunction. All animal use was approved by the Institutional Animal Care and Use Committee at the University of North Carolina at Chapel Hill. Mice lacking CHIP expression (*Stub1* targeted knockout, gene ID: 56424) B6;129-*Stub1*^{tm1Cpat}/Mmnc (RRID:MMRRC_037422-UNC) on a mixed background of 129S/SvEv and C57BL/6 were previously reported¹⁰. For this line, knockout mice are delineated (CHIP^{-/-}) and control animals are age and sex matched wildtype littermate controls (referred to as CHIP^{+/+}).

Generation of CHIP (*Stub1* gene) T247M mutant mice. *Guide RNA Cloning:* Guide RNA protospacer (target) sequences were cloned into a T7 promoter vector in context with guide RNA structural elements, allowing T7-mediated *in vitro* transcription to produce the full guide RNA molecule. A guanine was added to the 5' end of protospacer sequences that do not have a native 5' guanine to allow T7 *in vitro* transcription initiation. T7 ligation mixtures were transformed into Stellar competent cells. Miniprep DNA was sequence-verified. *Guide RNA In Vitro Transcription.* Guide RNA plasmids were linearized with DraI, purified by silica column (Qiaquick) and used as template for T7 *in vitro* transcription using the NEB HiScribe T7 kit. Reactions were performed at 37°C overnight as recommended by the manufacturer using 1000 ng linear guide RNA plasmid. After addition of DNase I for 30 min, guide RNAs were purified

using Qiagen RNEasy mini kit, eluted in 30 µl RNase-free microinjection buffer (5 mM Tris-Cl pH7.5, 0.1 mM EDTA) and quantitated on a Nanodrop spectrophotometer. *Guide RNA Activity Test:* The Cas9/guide RNA target region was PCR amplified from wild-type C57BL/6 DNA using primers Stub1-ScF1 (5'-GGAGACAGGAGTTGCCACACA-3') and Stub1-ScR1 (5'-CAGTTCAGAACCCATCAGCAGG-3'). PCR product was purified on a silica minicolumn and eluted in 10 mM Tris-Cl pH8.5. *In Vitro Cleavage Assay:* Guide RNAs were tested for activity in 1x NEB restriction buffer 3, 1 mg/ml BSA, 30 µg/ml Cas9 protein, 300 ng target DNA and 600 ng guide RNA in a 20 µl reaction volume. A control reaction was performed in parallel with all components except guide RNA. Reactions were incubated at 37°C for 1 hr followed by 80°C for 10 min, separated on 2% Agarose TAE gels and imaged using a standard ethidium bromide gel imaging system. Guide RNA Stub1-g82T (GAACCCTGCATTACACCCAGTGG, protospacer associated motif NGG underlined) produced nearly 100% target site cleavage. *Mouse production:* Genome editing was performed using CRISPR/Cas9 technology with the modification of mouse sequence NM_019719 at ntids #740 and #741 resulting in change of Threonine247 to Methionine (ACA to ATG). Founder animals were produced by microinjection of C57BL/6J embryos with a mixture of 100 ng/ul Cas9 mRNA, 50 ng/ul Stub1 guide RNA g82T and 100 ng/ul donor oligonucleotide Stub1-T247M-T (5'-TGACTACTTGTGTGGCAAGATTAGCTTTGAGCTGATGCGGGAACCCTGCATTATGCC CAGTGGTATCACCTATGACCGCAAGGACATTGAGGAGCACCTGCAGGTAAG-3') in 5 mM Tris pH7.5, 0.1 mM EDTA. Injected embryos were surgically implanted in CD-1 pseudopregnant recipients and resulting pups were genotyped by PCR amplification of the Stub1 T246 region followed by Sanger sequencing. Animals harboring the Stub1 T246M codon change were identified by deconvolution of sequence traces. Founder animals were mated to wild-type C57BL/6J animals and F1 animals harboring the T246M mutation were intercrossed to generate homozygous animals ((*Stub1* endonuclease-mediated mutation, gene ID: 56424) C57BL/6J-Stub11Schiz (MGI: 5883536)). For this line, knockin mice are delineated (CHIP^{M247/M247})

and control animals are age and sex matched wildtype littermate controls (referred to as CHIP^{T247/T247}). *Off-target analysis:* For off-target analysis, guide RNAs were checked for predicted off-target sites using the web server crispr.mit.edu. The top 10 predicted off-target sites were PCR amplified from the founder biopsy DNA and PCR products were sequenced to detect the presence of mutations at each off-target site. Mutations were detected based on the presence of multiple peaks in the sequence traces.

CHIP gene modified mice kidney sample preparation. Kidneys were homogenized in ice-cold isolation solution (250 mM sucrose, 10 mM triethanolamine, pH 7.6, containing the protease inhibitors leupeptin (1 mg/ml) and Pefa-block (0.1 mg/ml) (Roche Applied Science) and phosphatase inhibitor mixture tablets (PhosSTOP, Roche Diagnostics A/S)) for generation of SDS-PAGE gel samples.

Water intake analysis and plasma and urine collection in CHIP mouse models. CHIP^{-/-} or CHIP^{M247/M247} and their respective wild-type controls were used to measure water intake and plasma and urine osmolalities. Animals were housed in individual cages on a 12/12 light/dark cycle with free access to standard rodent chow (Teklad) and water. We used CHIP^{-/-} and CHIP^{M247/M247} mice with their respective wild-type controls, balanced for sex and age (average age of 5.5 mo, range 3 mo - 9 mo, n = 7 - 8 mice per genotype). For daily water intake measurements, mice were moved to a procedure room isolated from outside interference to minimize accidental water loss. Three cages with no mice were manipulated in the same manner and used to control for water loss due to evaporation or spilling due to handling. The initial weight of the water bottles was measured and then at the same time for three consecutive days thereafter. Daily water intake was calculated assuming density of water = 1 g/ml.

Spontaneous urines were collected from the same cohort of mice towards the end of the light cycle on three consecutive days for a total of three collections per mouse. Mice were held individually above a piece of parafilm until spontaneous voiding occurred (usually within 1 min). Urine was transferred to a micro-centrifuge tube and frozen at -20°C. Urine was centrifuged at 12,000 *g* for 10 min to remove precipitates before analysis. Mice were euthanized by way of carbon dioxide asphyxiation with a secondary method of vital organ collection. Blood plasma was prepared by collecting blood in BD Microtainer SST tubes (REF 365967). Urine and plasma osmolalities were measured using an Advanced Wide-Range Osmometer 3W2 (Advanced Instruments Inc., MA, USA). Sodium, potassium, chloride, urea and creatinine concentrations were measured in urine and plasma samples by the Clinical Pathology Laboratory at the Medical Research Council (Harwell, Oxfordshire, UK).

In vitro ubiquitylation reactions. Performed as previously described ¹¹. Briefly, 1 µM of bacterially-expressed Hsc70 was incubated in the presence of 2.5 µM CHIP, 1.6 µM of AQP2, 50 nM purified Ube1 (BostonBiochem, E305), 2.5 µM purified Ubch5c (BostonBiochem, E2-627) and 0.25 µM ubiquitin (BostonBiochem, U100H) in 50 mM Tris pH 7.5, 600 µM DTT, 2.5 mM MgCl₂-ATP (BostonBiochem, B20) in a total volume of 10 µl. Reactions were incubated for 1 h at 37 °C and stopped by 1:1 addition of 2X Laemmli sample buffer containing 5% β-mercaptoethanol and denatured at 100°C for 5 min. Samples were separated on a 4-15% Mini-PROTEAN® TGX Stain-Free™ Precast Gel at 150V and transferred to a PVDF membrane at 25V for 7 min using the Trans-Blot Turbo Transfer System (Bio-Rad). The membrane was blocked with 5% milk for 1 h at room temperature before immunoblotting with the appropriate primary antibodies: rabbit anti-AQP2 1:1,000 (H7661), rat anti-HSC70 1:5,000 (Enzo, ADI-SPA-815), mouse anti-CHIP 1:2,000 (Sigma, S1073) overnight at 4°C. Blots were then incubated for 1 h at room temperature with anti-mouse, anti-rabbit 1:10,000 (CST, 7076S and 7074S) or anti-

rat 1:10,000 (Sigma, A5795) IgG-HRP linked secondary antibodies and were developed using Clarity™ Western ECL Substrate (Bio-Rad) and imaged using the EC3™ Imaging System (UVP).

Statistics. For western blotting and mouse physiological recordings, data are expressed as mean±S.E.M. For two groups, data meeting the statistical assumptions of normality were assessed using an unpaired Student's *t*-test. Comparisons of more than two groups were performed using either a one-way ANOVA or two-way repeated-measures ANOVA followed by Student-Newman-Keuls or Tukey's multiple comparison tests, respectively. Significance was considered at $P < 0.05$. The researchers were not completely blinded during sample collection and data acquisition/analysis.

REFERENCES

1. Yang F, Shen Y, Camp DG, 2nd, Smith RD: High-pH reversed-phase chromatography with fraction concatenation for 2D proteomic analysis. *Expert Rev Proteomics* 9: 129-134, 2012
2. Hoffert JD, Pisitkun T, Saeed F, Song JH, Chou CL, Knepper MA: Dynamics of the G protein-coupled vasopressin V2 receptor signaling network revealed by quantitative phosphoproteomics. *Mol Cell Proteomics* 11: M111 014613, 2012
3. Meyer AH, Katona I, Blatow M, Rozov A, Monyer H: In vivo labeling of parvalbumin-positive interneurons and analysis of electrical coupling in identified neurons. *J Neurosci* 22: 7055-7064, 2002
4. Moeller HB, Aroankins TS, Slengerik-Hansen J, Pisitkun T, Fenton RA: Phosphorylation and ubiquitylation are opposing processes that regulate endocytosis of the water channel aquaporin-2. *J Cell Sci* 127: 3174-3183, 2014
5. Hoffert JD, Fenton RA, Moeller HB, Simons B, Tchapyjnikov D, McDill BW, Yu MJ, Pisitkun T, Chen F, Knepper MA: Vasopressin-stimulated increase in phosphorylation at Ser269

- potentiates plasma membrane retention of aquaporin-2. *J Biol Chem* 283: 24617-24627, 2008
6. Moeller HB, Knepper MA, Fenton RA: Serine 269 phosphorylated aquaporin-2 is targeted to the apical membrane of collecting duct principal cells. *Kidney Int* 75: 295-303, 2009
 7. Yu MJ, Miller RL, Uawithya P, Rinschen MM, Khositseth S, Braucht DW, Chou CL, Pisitkun T, Nelson RD, Knepper MA: Systems-level analysis of cell-specific AQP2 gene expression in renal collecting duct. *Proc Natl Acad Sci U S A* 106: 2441-2446, 2009
 8. Fenton RA, Brond L, Nielsen S, Praetorius J: Cellular and subcellular distribution of the type-2 vasopressin receptor in the kidney. *Am J Physiol Renal Physiol* 293: F748-760, 2007
 9. Moeller HB, Slengerik-Hansen J, Aroankins T, Assentoft M, MacAulay N, Moestrup SK, Bhalla V, Fenton RA: Regulation of the Water Channel Aquaporin-2 via 14-3-3theta and -zeta. *J Biol Chem* 291: 2469-2484, 2016
 10. Dai Q, Zhang C, Wu Y, McDonough H, Whaley RA, Godfrey V, Li HH, Madamanchi N, Xu W, Neckers L, Cyr D, Patterson C: CHIP activates HSF1 and confers protection against apoptosis and cellular stress. *EMBO J* 22: 5446-5458, 2003
 11. Jiang J, Ballinger CA, Wu Y, Dai Q, Cyr DM, Hohfeld J, Patterson C: CHIP is a U-box-dependent E3 ubiquitin ligase: identification of Hsc70 as a target for ubiquitylation. *J Biol Chem* 276: 42938-42944, 2001

SIGNIFICANCE STATEMENT

The distal convoluted tubule (DCT) and cortical collecting duct (CCD) play unique and diverse roles in water and electrolyte handling, but little is known about the unique subset of regulatory proteins in these cells. This manuscript combines proteomics and bioinformatics to identify differentially expressed proteins in the DCT and CCD under various physiological stimuli. The different regulatory proteins within each cell type likely infer their unique transport properties. We show that one regulatory protein highly expressed in the CCD, the E3 ubiquitin ligase CHIP, modulates the function of the water channel aquaporin-2 and plays a role in renal water handling. Pharmaceutical modulation of CHIP function could be a novel approach to treat various water balance disorders.